Westfälische Wilhelms-Universität Münster

Master's Thesis

Gradient Dynamics Approach to Chemically Reacting Sessile Liquid Drops

Submitted by:
Florian Alexander Voss

First examiner:
Prof. Dr. Uwe Thiele
Second examiner:
Priv. Doz. Dr. Svetlana Gurevich

September 12, 2023

Abstract

In the present thesis, a gradient dynamics approach to chemically reacting sessile liquid drops is presented. Based on the theory of non-equilibrium thermodynamics and the principle of detailed balance, it is shown how chemical systems can be written as a gradient dynamics. In contrast to the usual approach of linear phenomenological laws, the reactive fluxes must be related non-linearly to the variations of the underlying free energy functional to recover mass action type kinetics. As an application, we construct a gradient dynamics based model of non-equilibrium sessile liquid drops covered by reactive, insoluble surfactants. The surfactants engage in an autocatalytic reaction and may transition between the drop surface and the gas phase by evaporation and condensation. The surfactant gas phases are assumed to be chemostatted and thus the drop is permanently driven away from equilibrium by evaporation and condensation of the surfactants. A linear stability analysis of a flat film reveals different instability regimes in the plane spanned by the reaction rate and the driving force, including Hopf- and Turing-unstable regions. We then study the resulting intricate drop dynamics using numerical continuation methods and time simulations. Here we find, inter alia, the emergence of patterned surfactant distributions on the drop as well as different modes of drop oscillation. The oscillatory modes (axisymmetric, anti-axisymmetric and asymmetric with respect to parity) are classified by the dynamics of the drop center of mass. In addition, we report linearly stable (modulated) traveling drop states, appearing from drift-pitchfork bifurcations (of standing waves). Consequently, the model allows for the directional transport of bulk liquid as a result of spontaneous symmetry breaking.

Contents

1. Introduction

1.1 The Second Law of Thermodynamics, Active Systems and Chemical Reactions

From the spreading of a drop of ink in water to the formation of crystals - the second law of thermodynamics describes how macroscopic systems relax to the state of thermodynamic equilibrium, regardless of their microscopic makeup and the specific equilibrium state. Its power lies in its generality and it has played a fundamental role in the development of the theoretical understanding of nature far beyond its original scope. Among others, Planck's theory of black body radiation and Einstein's theory of spontaneous emission are both based on the second law of thermodynamics. For isolated systems, i.e., systems that can exchange neither matter nor energy with their environment, the second law of thermodynamics states the existence of a function, the entropy S, which can only increase in time ($\dot{S} \geq 0$). For systems which are not isolated, the second law still demands that the entropy production $\dot{S}_i$ due to internal processes cannot be negative ($\dot{S}_i \geq 0$). In addition, there now exists an external current of entropy $\dot{S}_e$ associated with the exchange of energy and matter (Fig. 1.1) and consequently the total rate of change of entropy $\dot{S} = \dot{S}_i + \dot{S}_e$ may be positive or negative.

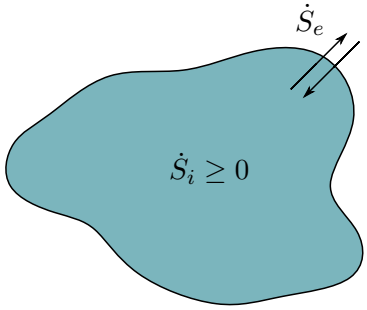

Figure 1.1: Any macroscopic system may experience an arbitrary change of entropy $\dot{S}_e$ due to exchange of energy and matter with its environment. However, the second law of thermodynamics requires that the entropy production $\dot{S}_i$ due to internal processes must be non-negative.

Nevertheless, even when an exchange of energy or both energy and matter is permitted (closed and open systems), the system may still evolve toward thermodynamic equilibrium under special conditions and there can still exist quantities that are analogous to the entropy in isolated systems. For instance, in closed systems at a constant temperature the Helmholz free energy F decreases monotonically as the system evolves toward equilibrium. Similarly, in open systems the grand potential Ω is minimized if the temperature, the pressure and the system volume are fixed. Such quantities, which show a monotonic increase or decrease in time and approach a maximum or minimum, are called Lyapunov-functions (or functionals). Their existence strongly restricts the possible paths a system can take as it evolves in time. However, inspection of the macroscopic world shows that many systems are subject to external gradients in temperature, pressure and chemical potentials which drive transport processes within the system. In a slightly more subtle manner, chemical potential gradients can also be applied not in three-dimensional space but in an abstract configuration space of chemical species where they then drive chemical reactions instead of diffusion. For systems which are exposed to such external gradients, it is usually found that the occuring processes are anything but monotonic since they do not relax to thermodynamic equilibrium. In fact, all biological systems must show time-periodic behavior since a fundamental aspect of life is cyclic reproduction. It is exactly this class of *active* systems, which are permanently out of equilibrium and for which usually no Lyapunov-function can be

found, that shows surprising self-organizing properties whose numerous aspects are still subject of research in biology, chemistry and physics.

In many such active systems, chemical reactions are present and they may enrich the resulting dynamics significantly. In fact, chemical reactions are often fundamental to the proper function of processes in living cells, ranging from the excitation and conduction of electric signals in axons [HH52] to the location of the cell center during cell division [BCR89]. Paradigmatic models of self-organization such as the Brusselator [Nic95] and the FitzHugh-Nagumo model [Fit61] have also emerged as abstractions of reacting systems found in nature. It should therefore come as no surprise that systems involving chemical reactions usually show strikingly complex behavior, particularly when driven away from equilibrium. However, regarding the emergent self-organizing behavior found in many such systems, it should not only be the aim to find and analyze characteristic model equations, such as the Brusselator, but to also study the transition to an active system. In this thesis, both aspects are treated. That is, the equations for chemical kinetics are first brought into a *gradient dynamics form* with a corresponding Lyapunov-functional. As an example, we then use a model for shallow liquid drops covered by reactive surfactants that can transition between the drop surface and the respective vapor phase by evaporation and condensation. The system is rendered active by chemostatting the vapor phases, i.e., by imposing a chemical potential gradient in the space of chemical species. This breaks the gradient dynamics form, leading to a non-equilibrium model that possesses rich behavior.

1.2 Outline

The structure of this thesis is as follows. In chapter 2, we present a gradient dynamics form of reaction-diffusion systems based on the theory of non-equilibrium thermodynamics. Here, we also discuss how active model systems like the Brusselator may be recovered from this structure. In chapter 3, thin liquid films covered by reactive surfactants are treated. First, we derive thermodynamic consistency conditions for such models from equilibrium considerations. Then, the dynamical equations are presented in a gradient dynamics form and some resulting cross-coupling effects between wetting phenomena and chemical reactions are briefly discussed. In chapter 4, we consider a model describing shallow drops covered by autocatalytically reacting surfactants. The system is driven away from equilibrium by evaporation and condensation of the surfactants. Here, we study the resulting dynamics in detail using the tools of linear stability analysis, time simulations and numerical continuation. Finally, the thesis is concluded in chapter 5 with a summary and an outlook.

2. Reaction-Diffusion Systems as Gradient Dynamics

In the following, a general structure of reaction-diffusion systems as gradient dynamics is derived from the theory of non-equilibrium thermodynamics and the assumption of detailed balanced mass action type kinetics. To considerable extent, the upcoming sections are based on the formalism of non-equilibrium thermodynamics presented in [SP84]. When suitable, the related chapters in [SP84] are indicated to supplement the present discussion. In Secs. 2.1 and 2.2, we review some basics of non-equilibrium thermodynamics. In Sec. 2.3, a gradient dynamics approach to reaction-diffusion systems is presented. In contrast to the usual linear phenomenological laws, the reactive fluxes must be related non-linearly to the variations of the underlying energy functional to obtain mass action type kinetics. In Secs. 2.4 to 2.6, we then give some applications of the presented formalism and it is discussed how active chemical systems may be recovered.

2.1 Conservation of Mass

Consider a spatially extended system comprising n components of mass density ρ_k, respectively. Between the components, $r \leq n-1$ independent chemical reactions may occur ([SP84], Ch. X). The corresponding balance equations for each component are

$$\frac{\partial \rho_k}{\partial t} = -\nabla \cdot (\rho_k \boldsymbol{v}_k) + \sum_{j=1}^{r} \nu_{kj} J_j, \tag{2.1}$$

where $\boldsymbol{v}_k$ is the velocity of componenent k. Partial time derivatives are denoted by $\partial/\partial t$ (abbreviated ∂_t) and we use $\nabla = (\partial_x, \partial_y, \partial_z)^{\mathrm{T}}$ in three dimensions. The quantity J_j represents the reactive flux of reaction j in terms of particles per unit volume and unit time. The coefficients ν_{kj} are products of the true stochiometric coefficients of component k in reaction j and the respective mass per particle m_k. For products of the reaction, ν_{kj} are counted positive, for educts negative. Because mass is conserved in each chemical reaction, the coefficients ν_{kj} obey the relation

$$\sum_{k=1}^{n} \nu_{kj} = 0 \tag{2.2}$$

for all reactions j. Introducing the barycentric (center of mass) velocity $\boldsymbol{v}$ and the diffusion flow $\boldsymbol{J}_k$ of component k

$$\boldsymbol{v} = \sum_{k=1}^{n} \rho_k \boldsymbol{v}_k / \rho, \tag{2.3}$$

$$\boldsymbol{J}_k = \rho_k \left(\boldsymbol{v}_k - \boldsymbol{v} \right) \tag{2.4}$$

with the total mass density

$$\rho = \sum_{k=1}^{n} \rho_k, \tag{2.5}$$

equation (2.1) can also be written as

$$\frac{\partial \rho_k}{\partial t} = -\nabla \cdot (\rho_k \boldsymbol{v}) - \nabla \cdot \boldsymbol{J}_k + \sum_{j=1}^{r} \nu_{kj} J_j. \tag{2.6}$$

Introducing the material derivative

$$\frac{\mathrm{d}}{\mathrm{d}t} = \frac{\partial}{\partial t} + \boldsymbol{v} \cdot \nabla, \tag{2.7}$$

we can also write equation (2.6) as

$$\frac{\mathrm{d}\rho_k}{\mathrm{d}t} = -\rho_k \nabla \cdot \boldsymbol{v} - \nabla \cdot \boldsymbol{J}_k + \sum_{j=1}^{r} \nu_{kj} J_j. \tag{2.8}$$

Note that the diffusion flows $\boldsymbol{J}_k$ are not independent and can be related by

$$\sum_{k=1}^{n} \boldsymbol{J}_k = 0. \tag{2.9}$$

This can be seen as a consequence of total mass conservation and will become relevant once the linear phenomenological laws are established. Alternatively, equations (2.1) and (2.6) can also be translated into time evolution equations for the particle number densities $n_k = \rho_k / m_k$ (abbreviated: particle densities) by division with the mass per particle m_k of component k:

$$\frac{\partial n_k}{\partial t} = -\nabla \cdot (n_k \boldsymbol{v}_k) + \sum_{j=1}^{r} \bar{\nu}_{kj} J_j \tag{2.10}$$

$$= -\nabla \cdot (n_k \boldsymbol{v}) - \nabla \cdot \bar{\boldsymbol{J}}_k + \sum_{j=1}^{r} \bar{\nu}_{kj} J_j. \tag{2.11}$$

The respective diffusion flows and true stochiometric coefficients are then given by

$$\bar{\boldsymbol{J}}_k = n_k \left(\boldsymbol{v}_k - \boldsymbol{v} \right), \tag{2.12}$$

$$\bar{\nu}_{kj} = \nu_{kj} / m_k. \tag{2.13}$$

Note that it does not generally hold that $\sum_{k=1}^{n} \bar{\boldsymbol{J}}_k = 0$ and $\sum_{k=1}^{n} \bar{\nu}_{kj} = 0$. This is in contrast to the mass diffusion flows $\boldsymbol{J}_k$ and the mass-associated stochiometric coefficients ν_{kj} which may therefore be seen as "more natural" quantities.

2.2 Entropy Balance Equation

The time evolution for $\boldsymbol{v}$ is given by

$$\rho \frac{\mathrm{d}\boldsymbol{v}}{\mathrm{d}t} = -\nabla \cdot \underline{\boldsymbol{P}} + \sum_{k=1}^{n} \rho_k \boldsymbol{F}_k, \tag{2.14}$$

where $\boldsymbol{F}_k$ is an external force per unit mass exerted on component k and $\underline{\boldsymbol{P}}$ is the stress tensor of the medium, which is assumed to be of the form

$$\underline{\boldsymbol{P}} = p \underline{\boldsymbol{U}} + \underline{\boldsymbol{\Pi}}. \tag{2.15}$$

Here, p is the scalar hydrostatic pressure and $\underline{\boldsymbol{U}}$ the three-dimensional unit tensor. Under the assumption of local thermodynamic equilibrium, a balance equation for the entropy density s (entropy per unit volume) can then be derived (cf. [SP84], Ch. III). In its most general form, it is given by

$$\frac{\partial s}{\partial t} = -\nabla \cdot \boldsymbol{J}_s + \sigma, \tag{2.16}$$

where the entropy flow $\boldsymbol{J}_s$ and the entropy source strength $\sigma \geq 0$ are given by

$$\boldsymbol{J}_s = \frac{1}{T}\left(\boldsymbol{J}_q - \sum_{k=1}^{n} \mu_k \boldsymbol{J}_k\right) + s\boldsymbol{v}, \tag{2.17}$$

$$\sigma = -\frac{1}{T^2}\boldsymbol{J}_q \cdot \nabla T - \frac{1}{T}\sum_{k=1}^{n} \boldsymbol{J}_k \cdot \left(T\nabla\left(\frac{\mu_k}{T}\right) - \boldsymbol{F}_k\right) - \frac{1}{T}\underline{\boldsymbol{\Pi}} : \nabla \boldsymbol{v} - \frac{1}{T}\sum_{j=1}^{r} J_j A_j. \tag{2.18}$$

In equations (2.17), (2.18), we introduced the heat flow $\boldsymbol{J_q}$, the specific chemical potential μ_k of substance k (chemical potential per unit mass) and the reaction affinities

$$A_j = \sum_{k=1}^{n} \nu_{kj}\mu_k \ , \quad (j = 1, \ldots, r). \tag{2.19}$$

The inner product of two real $m \times n$ matrices $\underline{\boldsymbol{A}} = (a_{ij}), \underline{\boldsymbol{B}} = (b_{ij})$ is defined as

$$\underline{\boldsymbol{A}} : \underline{\boldsymbol{B}} = \sum_{i=1}^{m}\sum_{j=1}^{n} a_{ij}b_{ij}. \tag{2.20}$$

The entropy flow and the entropy source strength can also be expressed in terms of the particle diffusion flows $\bar{\boldsymbol{J}}_k$, the chemical potentials per particle $\bar{\mu}_k = m_k\mu_k$ and the external forces per particle $\bar{\boldsymbol{F}}_k = m_k\boldsymbol{F}_k$:

$$\boldsymbol{J}_s = \frac{1}{T}\left(\boldsymbol{J}_q - \sum_{k=1}^{n} \bar{\mu}_k \bar{\boldsymbol{J}}_k\right) + s\boldsymbol{v}, \tag{2.21}$$

$$\sigma = -\frac{1}{T^2}\boldsymbol{J}_q \cdot \nabla T - \frac{1}{T}\sum_{k=1}^{n} \bar{\boldsymbol{J}}_k \cdot \left(T\nabla\left(\frac{\bar{\mu}_k}{T}\right) - \bar{\boldsymbol{F}}_k\right) - \frac{1}{T}\underline{\boldsymbol{\Pi}} : \nabla \boldsymbol{v} - \frac{1}{T}\sum_{j=1}^{r} J_j A_j. \tag{2.22}$$

Similarly, the affinities can be written in terms of particle number quantities, since

$$A_j = \sum_{k=1}^{n} \nu_{kj}\mu_k = \sum_{k=1}^{n} \bar{\nu}_{kj}\bar{\mu}_k \ , \quad (j = 1, \ldots, r). \tag{2.23}$$

2.3 Reaction-Diffusion Systems

To apply the previously described formalism to reaction-diffusion-type systems, an isotropic system in thermal equilibrium with a heat bath without any external forces will be considered. Consequently, the temperature T will be treated as uniform and constant. Viscous phenomena will also be neglected. In this case, the entropy production (2.22) reduces to

$$\sigma = -\frac{1}{T}\sum_{k=1}^{n} \bar{\boldsymbol{J}}_k \cdot (\nabla \bar{\mu}_k) - \frac{1}{T}\sum_{j=1}^{r} J_j A_j. \tag{2.24}$$

For simplicity, the barycentric velocity $\boldsymbol{v}$ will be assumed negligible. This approximation is valid, for instance, when the masses m_k of the individual components do not differ greatly (cf. [SP84], Ch. XI, §4) and the system is sufficiently close to mechanical equilibrium.[1] Then, the flux $\bar{\boldsymbol{J}}_k$ reduces to

$$\bar{\boldsymbol{J}}_k = n_k \boldsymbol{v}_k \tag{2.25}$$

[1] For the case of actual mechanical equilibrium, Prigogine [Pri47] has shown that the diffusion flow $\bar{\boldsymbol{J}}_k$ in the entropy production can be replaced by any flow

$$\bar{\boldsymbol{J}}_k^a = n_k(\boldsymbol{v}_k - \boldsymbol{v}^a),$$

where $\boldsymbol{v}^a$ is an arbitrary reference velocity. Therefore, assuming mechanical equilibrium, one may also assume any other characteristic velocity of the system to be negligible. This leads to the same time evolution equations for the particle densities but imposes further restrictions on the phenomenological coefficients. Here, we will simply assume that contributions of the barycentric velocity are comparatively small, i.e., $||\boldsymbol{v}|| \ll ||\boldsymbol{v}_k||$.

and the time evolution equation (2.10) can be written as

$$\frac{\partial n_k}{\partial t} = -\nabla \cdot \bar{\boldsymbol{J}}_k + \sum_{j=1}^{r} \bar{\nu}_{kj} J_j. \tag{2.26}$$

For the diffusive flows, we assume linear phenomenological laws of the form

$$\bar{\boldsymbol{J}}_i = -\frac{1}{T} \sum_{k=1}^{n} L_{ik} \nabla \bar{\mu}_k = -\sum_{k=1}^{n} \tilde{L}_{ik} \nabla \bar{\mu}_k \tag{2.27}$$

with $\tilde{L}_{ik} = L_{ik}/T$. This approximation is fully consistent with (2.24). In fact, the first term of the entropy production (2.24) is valid only as long as the linear law (2.27) holds (cf. [SP84], Ch. X, §2). Furthermore, the Onsager matrix $\underline{\boldsymbol{L}} = (L_{ik})_{i,k}$ must be symmetric and positive semi-definite to account for microscopic reversibility as well as non-negative entropy production [Ons31a; Ons31b]. Lastly, because of the linear relation between the diffusive flows (2.9) which may be reformulated as

$$\sum_{k=1}^{n} m_k \bar{\boldsymbol{J}}_k = 0, \tag{2.28}$$

the Onsager coefficients must fulfill the relations

$$\sum_{k=1}^{n} m_k \tilde{L}_{ik} = 0, \tag{2.29}$$

$$\sum_{i=1}^{n} m_i \tilde{L}_{ik} = 0 \tag{2.30}$$

as a consequence of mass conservation (cf. [SP84], Ch. VI, §3). For chemical reactions, linear relationships between the fluxes J_j and the conjugated forces $-A_j/T$ in (2.24) are generally insufficient ([SP84], Ch. X, §2). Therefore, the reactive fluxes J_j are assumed to obey generalized mass action type kinetics of the form

$$J_j = J_j^+ - J_j^- = k_j^+ \prod_{\bar{\nu}_{kj}<0} \lambda_k^{-\bar{\nu}_{kj}} - k_j^- \prod_{\bar{\nu}_{kj}>0} \lambda_k^{\bar{\nu}_{kj}}, \tag{2.31}$$

where λ_k are the activities of the individual components with

$$\lambda_k = e^{\frac{\bar{\mu}_k}{k_b T}}. \tag{2.32}$$

Here, k_b is the Boltzmann constant. For ideal gas reactions, it has been shown that equation (2.31) ensures maximum consistency with the second term of (2.24) [RM61; SP84]. In addition, we now use that the principle of detailed balance holds, i.e., that at equilibrium the total reactive fluxes J_j of each reaction must vanish *separately*.[2] This is equivalent to

$$J_j^{+,\mathrm{eq}} = J_j^{-,\mathrm{eq}}. \tag{2.33}$$

The principle of detailed balance is a direct extension of microscopic reversibility [Gor14; SP84] and therefore ensures that dynamics of the form (2.31) relax to *actual* thermodynamic equilibrium. Note that this is not ensured by assuming (2.31) since for multiple reactions the resulting

[2]Naturally, a similar condition must also hold for transport processes like diffusion, i.e., $\nabla \bar{\mu}_i^{\mathrm{eq}} = 0$ at equilibrium. However, if the Onsager matrix is actually positive-definite instead of only positive semi-definite, as is usually the case, this is ensured since then the entropy production only vanishes if this condition is fulfilled (cf. the first term of equation (2.49)).

kinetics may exhibit non-equilibrium steady states that violate (2.33), as first discussed by Wegscheider [Weg02]. Introducing (2.31) into (2.33) yields

$$k_j^+ \exp\left(-\sum_{\bar{v}_{kj}<0} \frac{\bar{v}_{kj}\bar{\mu}_k^{\mathrm{eq}}}{k_b T}\right) = k_j^- \exp\left(\sum_{\bar{v}_{kj}>0} \frac{\bar{v}_{kj}\bar{\mu}_k^{\mathrm{eq}}}{k_b T}\right). \tag{2.34}$$

Since the affinities $A_j = \sum_{k=1}^n \bar{\nu}_{kj}\bar{\mu}_k$ must vanish at equilibrium, we thus obtain from (2.34) the condition

$$k_j^+ = k_j^- \equiv k_j. \tag{2.35}$$

By considering (2.35), the mass action kinetics (2.31) can then be re-expressed as

$$J_j = J_j^+ - J_j^- = k_j \left[\exp\left(-\sum_{\bar{\nu}_{kj}<0} \frac{\bar{\nu}_{kj}\bar{\mu}_k}{k_b T}\right) - \exp\left(\sum_{\bar{\nu}_{kj}>0} \frac{\bar{\nu}_{kj}\bar{\mu}_k}{k_b T}\right)\right], \tag{2.36}$$

which is referred to by some authors as "standard equation of chemical kinetics" [BEK78]. Equation (2.36) has two notable special cases. Firstly, we assume an ideal mixture with the chemical potentials given by

$$\bar{\mu}_k = k_b T \ln\left(n_k a_k^3\right) + \zeta_k(T). \tag{2.37}$$

Here, $a_k > 0$ denote some characteristic length scales of the individual species and $\zeta_k(T)$ represents a general temperature dependence of the chemical potentials. For simplicity of notation, it will now be assumed that $a_k = 1$ in suitable units, without loss of generality. We may then also write

$$\bar{\mu}_k = k_b T \ln\left(n_k\right) + \zeta_k(T). \tag{2.38}$$

By inserting (2.38) into (2.36), the well-known mass action kinetics

$$J_j = k_j^f \prod_{\bar{\nu}_{kj}<0} n_k^{-\bar{\nu}_{kj}} - k_j^b \prod_{\bar{\nu}_{kj}>0} n_k^{\bar{\nu}_{kj}} \tag{2.39}$$

with the reaction constants

$$k_j^f = k_j \exp\left(-\sum_{\bar{\nu}_{kj}<0} \frac{\bar{\nu}_{kj}\zeta_k}{k_b T}\right), \tag{2.40}$$

$$k_j^b = k_j \exp\left(\sum_{\bar{\nu}_{kj}>0} \frac{\bar{\nu}_{kj}\zeta_k}{k_b T}\right) \tag{2.41}$$

are then recovered. Because of (2.35), detailed balance is ensured in this case. Secondly, (2.36) can be re-written as

$$J_j = k_j \exp\left(-\sum_{\bar{\nu}_{kj}<0} \frac{\bar{\nu}_{kj}\bar{\mu}_k}{k_b T}\right)\left[1 - \exp\left(\frac{A_j}{k_b T}\right)\right]. \tag{2.42}$$

Then, close to chemical equilibrium ($A_j \ll k_b T$), expanding (2.42) to first order yields

$$J_j = -k_j \exp\left(-\sum_{\bar{\nu}_{kj}<0} \frac{\bar{\nu}_{kj}\bar{\mu}_k^{\mathrm{eq}}}{k_b T}\right)\frac{A_j}{k_b T}, \tag{2.43}$$

which corresponds to linear laws for the reactive fluxes close to chemical equilibrium.

In total, the time evolution (2.26) of the individual particle densities n_k is now given by

$$\frac{\partial n_k}{\partial t} = \sum_{i=1}^n \nabla \cdot \left(\tilde{L}_{ki}\nabla\bar{\mu}_i\right) + \sum_{j=1}^r \bar{\nu}_{kj} J_j, \tag{2.44}$$

where the linear laws (2.27) were used and J_j are given by (2.36). It is important to note that by assuming detailed balance (2.35) the dynamics (2.44) is guaranteed to exhibit another thermodynamic property, namely monotonic relaxation toward equilibrium. This can be seen by defining a Gibbs functional G which is related to the chemical potentials by

$$\bar{\mu}_k = \frac{\delta G}{\delta n_k}, \tag{2.45}$$

where $\delta G/\delta n_k$ denotes the functional derivative of G with respect to n_k. The total derivative of G is then given by[3]

$$\begin{aligned}
\frac{\mathrm{d}G}{\mathrm{d}t} &= \int \mathrm{d}\boldsymbol{x} \left[\sum_{k=1}^{n} \frac{\delta G}{\delta n_k} \frac{\partial n_k}{\partial t} \right] && (2.46)\\
&= \int \mathrm{d}\boldsymbol{x} \left[\sum_{k=1}^{n} \frac{\delta G}{\delta n_k} \left(\sum_{i=1}^{n} \nabla \cdot \left(\tilde{L}_{ki} \nabla \frac{\delta G}{\delta n_i} \right) + \sum_{j=1}^{r} \bar{\nu}_{kj} J_j \right) \right] && (2.47)\\
&= -\int \mathrm{d}\boldsymbol{x} \left[\sum_{i,k=1}^{n} \tilde{L}_{ki} \left(\nabla \frac{\delta G}{\delta n_k} \right) \cdot \left(\nabla \frac{\delta G}{\delta n_i} \right) \right] + \sum_{j=1}^{r} \int \mathrm{d}\boldsymbol{x} \left(J_j^+ - J_j^- \right) \sum_{k=1}^{n} \left[\frac{\delta G}{\delta n_k} \bar{\nu}_{kj} \right] && (2.48)\\
&= -\int \mathrm{d}\boldsymbol{x} \left[\sum_{i,k=1}^{n} \tilde{L}_{ki} \left(\nabla \frac{\delta G}{\delta n_k} \right) \cdot \left(\nabla \frac{\delta G}{\delta n_i} \right) \right] + k_b T \sum_{j=1}^{r} \int \mathrm{d}\boldsymbol{x} \left(J_j^+ - J_j^- \right) \ln \left(\frac{J_j^-}{J_j^+} \right) && (2.49)\\
&\leq 0. && (2.50)
\end{aligned}$$

The integration domain is the whole system. From (2.47) to (2.48), partial integration was performed on the first term (assuming e.g. no-flux boundary conditions) and the definition (2.36) of J_j was used in the second term. From (2.48) to (2.49), the actual expression for J_j, also given by (2.36), was used. Note that this step is only possible because of the common coefficient k_j due to detailed balance. The final inequality follows from the positive semi-definiteness of the Onsager matrix and from the observation that the factors in the second term have opposite signs, always. Therefore, G is a Lyapunov-functional for (2.44) with its minimum corresponding to thermodynamic equilibrium.[4] Oscillatory dynamics, as found in many active systems, may then be enabled by permitting or modifying fluxes across the system boundaries or allowing for irreversible reactions (detailed balance excludes this directly). Often, these fluxes are implied by keeping certain reactant concentrations constant [KZ21; Zwi22]. For the well-known example of the Brusselator (cf. [Nic95]), irreversible reactions are assumed together with constancy of certain concentrations, for instance. In this case, it is therefore unsurprising that oscillatory behavior can be observed.

We remark that non-monotonic behavior can also occur in passive systems if the Onsager relations are violated. Then, the phenomenological matrix is the superposition of a symmetric and an anti-symmetric part, where the anti-symmetric part corresponds to energy-conserving processes which do not contribute to $\mathrm{d}G/\mathrm{d}t$. As a consequence, damped oscillations of the pertinent energy functional may then be observed as the system relaxes towards equilibrium [Hei17]. Cases in which the Onsager relations do not hold include non-ergodic systems [BB18], where it has been shown that inertia may trigger non-ergodicity [Che+21].

[3] A similar proof for the entropy can be found in [Gas22].

[4] Note that the principle of detailed balance is not *necessary* for the existence of a Lyapunov-function in homogeneous/well-mixed mass action type kinetics. In fact, there exists a wider class of "complex balanced" systems that are guaranteed to relax to (non-equilibrium) steady states in this manner [HJ72; Fei72; Fei87]. Systems that fulfill the principle of detailed balance and therefore relax to *thermodynamic* equilibrium belong to this class, too.

2.4 Example: Ideal Ternary Mixture of Reacting Components with Diffusion

As a first, simple example of (2.44), an ideal mixture of three reacting components will be considered. The Gibbs functional is given by

$$G = \int \sum_{i=1}^{3} k_b T n_i \left[\ln\left(n_i a_i^3\right) - 1 + \zeta_i(T)/k_b T \right] \mathrm{d}\boldsymbol{x}. \tag{2.51}$$

Again, n_i denote the particle densities of each chemical species (particles per unit volume) and $\zeta_i(T)$ represents some general temperature dependence of the chemical potentials. For the characteristic scales $a_i > 0$, we again assume without loss of generality that $a_i = 1$ in suitable units and then write the chemical potentials as

$$\bar{\mu}_k = \frac{\delta G}{\delta n_k} = k_b T \ln\left(n_k\right) + \zeta_k(T). \tag{2.52}$$

Furthermore, only one chemical reaction of the form

$$|\bar{\nu}_1| N_1 + |\bar{\nu}_2| N_2 \leftrightharpoons \bar{\nu}_3 N_3 \tag{2.53}$$

may take place. Here, $\bar{\nu}_{1,2}$ are taken to be negative. We now specify the Onsager matrix as

$$\underline{\tilde{\boldsymbol{L}}} = \begin{pmatrix} \tilde{D}_1 n_1 & 0 & -\frac{m_1}{m_3}\tilde{D}_1 n_1 \\ 0 & \tilde{D}_2 n_2 & -\frac{m_2}{m_3}\tilde{D}_2 n_2 \\ -\frac{m_1}{m_3}\tilde{D}_1 n_1 & -\frac{m_2}{m_3}\tilde{D}_2 n_2 & \frac{m_1^2}{m_3^2}\tilde{D}_1 n_1 + \frac{m_2^2}{m_3^2}\tilde{D}_2 n_2 \end{pmatrix} \tag{2.54}$$

$$\approx \begin{pmatrix} \tilde{D}_1 n_1 & 0 & -\tilde{D}_1 n_1 \\ 0 & \tilde{D}_2 n_2 & -\tilde{D}_2 n_2 \\ -\tilde{D}_1 n_1 & -\tilde{D}_2 n_2 & \tilde{D}_1 n_1 + \tilde{D}_2 n_2 \end{pmatrix} \tag{2.55}$$

with $\tilde{D}_i > 0$ as constants. Note that (2.54) fulfills the mass conservation constraints (2.29) and (2.30). For simplicity, from (2.54) to (2.55) all masses were assumed equal.[5] The time evolution equations (2.44) then read

$$\frac{\partial n_1}{\partial t} = D_1 \Delta n_1 - \nabla \cdot \left(D_1 \frac{n_1}{n_3} \nabla n_3 \right) + \bar{\nu}_1 \left(k_f n_1^{-\bar{\nu}_1} n_2^{-\bar{\nu}_2} - k_b n_3^{\bar{\nu}_3} \right), \tag{2.57}$$

$$\frac{\partial n_2}{\partial t} = D_2 \Delta n_2 - \nabla \cdot \left(D_2 \frac{n_2}{n_3} \nabla n_3 \right) + \bar{\nu}_2 \left(k_f n_1^{-\bar{\nu}_1} n_2^{-\bar{\nu}_2} - k_b n_3^{\bar{\nu}_3} \right), \tag{2.58}$$

$$\frac{\partial n_3}{\partial t} = -D_1 \Delta n_1 - D_2 \Delta n_2 + \nabla \cdot \left(D_1 \frac{n_1}{n_3} \nabla n_3 + D_2 \frac{n_2}{n_3} \nabla n_3 \right) + \bar{\nu}_3 \left(k_f n_1^{-\bar{\nu}_1} n_2^{-\bar{\nu}_2} - k_b n_3^{\bar{\nu}_3} \right), \tag{2.59}$$

where the rate coefficients are given by

$$k_f = k e^{-\frac{\bar{\nu}_1 \zeta_1 + \bar{\nu}_2 \zeta_2}{k_b T}}, \tag{2.60}$$

$$k_b = k e^{\frac{\bar{\nu}_3 \zeta_3}{k_b T}}, \tag{2.61}$$

[5] In this case, the sum over all true stochiometric coefficients must vanish because (2.2) can then be divided by the mass per particle m such that

$$\sum_{k=1}^{n} \bar{\nu}_{kj} = 0. \tag{2.56}$$

Therefore, if one starts with a given set of true stochiometric coefficients, i.e., by considering a specific chemical reaction, it may be invalid to assume that the particle masses of all components are equal.

with $k > 0$. The diffusion coefficients $D_{1,2}$ are

$$D_{1,2} = k_b T \tilde{D}_{1,2}. \tag{2.62}$$

Note that the mixed densities $q_1 = \bar{\nu}_3 n_1 + |\bar{\nu}_1| n_3$ and $q_2 = \bar{\nu}_3 n_2 + |\bar{\nu}_2| n_3$, or equivalently[6] the total particle density $n = n_1 + n_2 + n_3$ and either q_1 or q_2, correspond to *independent* conservation laws in Eqs. (2.57)-(2.59). For central results and further interesting phenomena related to (active) reaction-diffusion systems with conservation laws, we refer to [HF18; Bra+21] and [CGA22]. For active (reaction-diffusion) systems with two conservation laws in particular, we also refer to [FT23] and the related discussion of different types of instabilities in Sec. 4.2.

2.5 Example: Heterogeneous Ternary Mixture of Reacting Components

The foregoing example can easily be generalized to non-ideal mixtures in heterogeneous systems. The corresponding Gibbs functional is chosen as

$$G = \int \sum_{i=1}^{3} \left(k_b T n_i \left[\ln\left(n_i a_i^3\right) - 1 + \zeta_i(T)/k_b T \right] + \frac{\kappa_i}{2} \left(\nabla n_i\right)^2 + \alpha_i n_{i-1} n_{i+1} \right) \mathrm{d}\boldsymbol{x}, \tag{2.63}$$

where and $\kappa_i, \alpha_i \geq 0$ are constants that represent an interfacial energy contribution and a Flory-Huggins interaction parameter [Hug41; Flo42], respectively. For compactness of notation, we now interpret the indices as cyclic such that, for instance, for $i = 3$ we have $i - 1 = 2$ and $i + 1 = 1$. We again assume $a_i = 1$ in suitable units and consequently obtain the chemical potentials

$$\bar{\mu}_k = \frac{\delta G}{\delta n_k} = k_b T \ln\left(n_k\right) + \zeta_k - \kappa_k \Delta n_k + \alpha_{k-1} n_{k-2} + \alpha_{k+1} n_{k+2}, \tag{2.64}$$

with the Laplace-Operator $\Delta = \partial_x^2 + \partial_y^2 + \partial_z^2$. The time evolution of the particle densities is now given by

$$\frac{\partial n_k}{\partial t} = \sum_{i=1}^{3} \nabla \cdot \left(\tilde{L}_{ki} \nabla \left[k_b T \ln\left(n_i\right) + \zeta_i - \kappa_i \Delta n_i + \alpha_{i-1} n_{i-2} + \alpha_{i+1} n_{i+2} \right] \right) \tag{2.65}$$

$$+ \bar{\nu}_k \left(k_f n_1^{-\bar{\nu}_1} n_2^{-\bar{\nu}_2} - k_b n_3^{\bar{\nu}_3} \right), \tag{2.66}$$

where the Onsager matrix (2.55) is used again. The rate coefficients now read

$$k_f = k \exp\left(-\frac{\bar{\nu}_1 \left[\zeta_1 - \kappa_1 \Delta n_1 + \alpha_2 n_3 + \alpha_3 n_2\right] + \bar{\nu}_2 \left[\zeta_2 - \kappa_2 \Delta n_2 + \alpha_1 n_3 + \alpha_3 n_1\right]}{k_b T} \right), \tag{2.67}$$

$$k_b = k \exp\left(\frac{\bar{\nu}_3 \left[\zeta_3 - \kappa_3 \Delta n_3 + \alpha_1 n_2 + \alpha_2 n_1\right]}{k_b T} \right). \tag{2.68}$$

Therefore, the reaction rates now depend on the local species densities and their curvatures and may thus vary greatly in the vicinity of interfaces. Additionally, it has been shown that chemical reactions reduce the complexity of phase diagrams [Zwi22], i.e., a heterogeneous binary mixture with a simple conversion reaction is incapable of phase separation since only the total mass is conserved, that is, there exists only one conservation law instead of two. Then, the Gibbs

[6] Because of mass conservation in chemical reactions and the additional assumption of equal masses per particle $m_k = m$, it follows that in this particular case, the sum over all *true* stochiometric coefficients must vanish, i.e. $\bar{\nu}_1 + \bar{\nu}_2 + \bar{\nu}_3 = 0$. Using this relation to re-express $\bar{\nu}_3$ in terms of $\bar{\nu}_{1,2}$ we then obtain $q_1 + q_2 = (|\bar{\nu}_1| + |\bar{\nu}_2|)n$. Therefore, equations (2.57)-(2.59) may be rewritten in terms of q_1, q_2 and n_3 or equivalently in terms of n, n_3 and either q_1 or q_2, where now two of the three equations are continuity equations. The system therefore has two independent conservation laws.

energy G can be minimized *locally*. Similarly, for the case of a heterogeneous ternary mixture it was shown that the presence of a conversion reaction reduces the equilibrium states to phase separation of a binary fluid as there are now only two conservation laws [Zwi22]. The same result must hold for the present example since, for instance, the densities $n = n_1 + n_2 + n_3$ and $q_1 = \bar{\nu}_3 n_1 + |\bar{\nu}_2| n_3$ correspond to independently conserved quantities.

2.6 Example: The Brusselator

Up to now, we have discussed two examples that lie completely within the presented formalism of equations (2.36) and (2.44). However, it is also of interest to understand in which ways property (2.50) can be broken to produce non-monotonic dynamics. To this end, we here derive the well-known reaction-diffusion equations of the Brusselator (cf. [Nic95], Ch. 2.6), starting from equations (2.36) and (2.44) with proper mass conservation (2.28). The underlying thermodynamic constraints are then relaxed in separate, explicit steps to make clear which additional assumptions are necessary to obtain standard reaction-diffusion systems that show self-organizing behavior.

In total, a system comprising six components is considered. Between the components, four chemical reactions take place for which the reaction equations are given by

$$N_3 \leftrightharpoons N_1, \tag{2.69}$$

$$N_4 + N_1 \leftrightharpoons N_2 + N_5, \tag{2.70}$$

$$2N_1 + N_2 \leftrightharpoons 3N_1, \tag{2.71}$$

$$N_1 \leftrightharpoons N_6. \tag{2.72}$$

In (2.69) to (2.72), chemical reactions going from left to right are defined as forward reactions. Therefore, species appearing on the right hand side of equations (2.69) to (2.72) correspond to positive stochiometric coefficients. Again, we assume an ideal system so that the Gibbs functional is given by

$$G = \int \sum_{i=1}^{3} k_b T n_i \left[\ln\left(n_i a_i^3\right) - 1 + \zeta_i(T)/k_b T \right] \, \mathrm{d}\boldsymbol{x}, \tag{2.73}$$

where $a_i > 0$ are characteristic length scales of each chemical species and $\zeta_i(T)$ denotes some general temperature dependence of the chemical potentials. For simplicity of notation, we again assume without loss of generality that $a_i = 1$ in suitable units and can then write the chemical potentials as

$$\bar{\mu}_k = \frac{\delta G}{\delta n_k} = k_b T \ln\left(n_k\right) + \zeta_k(T). \tag{2.74}$$

Accounting for mass conservation, we specify the Onsager matrix as

$$\underline{\tilde{\boldsymbol{L}}} = \begin{pmatrix} \tilde{D}_1 n_1 & 0 & 0 & 0 & 0 & -\tilde{D}_1 n_1 \\ 0 & \tilde{D}_2 n_2 & 0 & 0 & 0 & -\tilde{D}_2 n_2 \\ 0 & 0 & \tilde{D}_3 n_3 & 0 & 0 & -\tilde{D}_3 n_3 \\ 0 & 0 & 0 & \tilde{D}_4 n_4 & 0 & -\tilde{D}_4 n_4 \\ 0 & 0 & 0 & 0 & \tilde{D}_5 n_5 & -\tilde{D}_5 n_5 \\ -\tilde{D}_1 n_1 & -\tilde{D}_2 n_2 & -\tilde{D}_3 n_3 & -\tilde{D}_4 n_4 & -\tilde{D}_5 n_5 & \sum_{k=1}^{5} \tilde{D}_k n_k \end{pmatrix}, \tag{2.75}$$

with $\tilde{D}_i > 0$ as constants. Note that in (2.75) we have again assumed equal masses per particle for all species. Because in (2.69) to (2.72) the sum of all *true* stochiometric coefficients vanishes for each reaction, this does not violate mass conservation (2.2). The reactive fluxes are given by (2.36). In total, the time evolution of the particle densities n_k is again determined by (2.44).

Now, we assume that the densities of components 3, 4, 5 and 6 are fixed (uniform and constant), e.g., with the use of some chemostat. This directly breaks the detailed balance condition (2.35) and the system cannot relax to thermodynamic equilibrium. For instance, the reactive flux of (2.70) is given by

$$J_2 = k_2 \exp\left[\frac{\bar{\mu}_4 + \bar{\mu}_1}{k_b T}\right] - k_2 \exp\left[\frac{\bar{\mu}_2 + \bar{\mu}_5}{k_b T}\right]. \tag{2.76}$$

Assuming fixed densities for components 3 to 6 implies however that the corresponding ideal chemical potentials are uniform and constant, too. Therefore J_2 is now given by

$$J_2 = k_2' \exp\left[\frac{\bar{\mu}_1}{k_b T}\right] - k_2'' \exp\left[\frac{\bar{\mu}_2}{k_b T}\right] \tag{2.77}$$

with

$$k_2' = k_2 \exp\left[\frac{\bar{\mu}_4^0}{k_b T}\right], \tag{2.78}$$

$$k_2'' = k_2 \exp\left[\frac{\bar{\mu}_5^0}{k_b T}\right], \tag{2.79}$$

where the chemical potentials $\bar{\mu}_4^0, \bar{\mu}_5^0$ are given by

$$\bar{\mu}_4^0 = k_b T \ln\left(n_4^0\right) + \zeta_4(T), \tag{2.80}$$

$$\bar{\mu}_5^0 = k_b T \ln\left(n_5^0\right) + \zeta_5(T). \tag{2.81}$$

Here, n_4^0 and n_5^0 denote the initial densities of components 4 and 5. From (2.78) and (2.79), it thus follows that detailed balance is broken since

$$k_2^+ = k_2' \neq k_2'' = k_2^-, \tag{2.82}$$

where $k_j^\pm$ are the rate constants of the general mass action type kinetics (2.31). This argument also holds for the other reactions in which some component densities are fixed. Note that once detailed balance is not fulfilled, the proof shown in (2.46) to (2.50) breaks down in line (2.49) since the prefactors k_j^+ and k_j^- occurring in J_j^+ and J_j^- need to be equal.

The assumption of fixed densities n_3, n_4, n_5 and n_6 implies corresponding in- and outfluxes everywhere in the system. Therefore, the time evolution equations of all component densities

now read[7]

$$\frac{\partial n_1}{\partial t} = \sum_{i=1}^{6} \nabla \cdot \left(\tilde{L}_{1i} \nabla \bar{\mu}_i \right) + \sum_{j=1}^{4} \bar{\nu}_{1j} J_j, \tag{2.83}$$

$$\frac{\partial n_2}{\partial t} = \sum_{i=1}^{6} \nabla \cdot \left(\tilde{L}_{2i} \nabla \bar{\mu}_i \right) + \sum_{j=1}^{4} \bar{\nu}_{2j} J_j, \tag{2.84}$$

$$\frac{\partial n_3}{\partial t} = \sum_{i=1}^{6} \nabla \cdot \left(\tilde{L}_{3i} \nabla \bar{\mu}_i \right) + \sum_{j=1}^{4} \bar{\nu}_{3j} J_j + J_c^3 = 0, \tag{2.85}$$

$$\frac{\partial n_4}{\partial t} = \sum_{i=1}^{6} \nabla \cdot \left(\tilde{L}_{4i} \nabla \bar{\mu}_i \right) + \sum_{j=1}^{4} \bar{\nu}_{4j} J_j + J_c^4 = 0, \tag{2.86}$$

$$\frac{\partial n_5}{\partial t} = \sum_{i=1}^{6} \nabla \cdot \left(\tilde{L}_{5i} \nabla \bar{\mu}_i \right) + \sum_{j=1}^{4} \bar{\nu}_{5j} J_j + J_c^5 = 0, \tag{2.87}$$

$$\frac{\partial n_6}{\partial t} = \sum_{i=1}^{6} \nabla \cdot \left(\tilde{L}_{6i} \nabla \bar{\mu}_i \right) + \sum_{j=1}^{4} \bar{\nu}_{6j} J_j + J_c^6 = 0. \tag{2.88}$$

Here, the fluxes J_c^k represent the action of the external chemostat and lead to vanishing temporal derivatives of the densities n_3, n_4, n_5 and n_6 at all points in the system. Therefore, the system of equations (2.83) to (2.88) can be reduced to

$$\frac{\partial n_1}{\partial t} = \sum_{i=1}^{2} \nabla \cdot \left(\tilde{L}_{1i} \nabla \bar{\mu}_i \right) + \sum_{j=1}^{4} \bar{\nu}_{1j} J_j, \tag{2.89}$$

$$\frac{\partial n_2}{\partial t} = \sum_{i=1}^{2} \nabla \cdot \left(\tilde{L}_{2i} \nabla \bar{\mu}_i \right) + \sum_{j=1}^{4} \bar{\nu}_{2j} J_j. \tag{2.90}$$

Now the transport terms in (2.89) and (2.90) contain only contributions from components 1 and 2 since all other chemical potentials are fixed. Therefore, the Onsager matrix (2.75) can be reduced to the effective matrix

$$\underline{\tilde{\boldsymbol{L}}}_{\text{eff}} = \begin{pmatrix} \tilde{D}_1 n_1 & 0 \\ 0 & \tilde{D}_2 n_2 \end{pmatrix} \tag{2.91}$$

which no longer fulfills relations (2.29) and (2.30). This, too, is a consequence of imposing the fluxes J_c^k, thus breaking total mass conservation. As a preliminary result, we obtain the time evolution equations

$$\frac{\partial n_1}{\partial t} = D_1 \Delta n_1 + k_1^f - k_1^b n_1 - k_2^f n_1 + k_2^b n_2 + k_3^f n_1^2 n_2 - k_3^b n_1^3 - k_4^f n_1 + k_4^b, \tag{2.92}$$

$$\frac{\partial n_2}{\partial t} = D_2 \Delta n_2 + k_2^f n_1 - k_2^b n_2 - k_3^f n_1^2 n_2 + k_3^b n_1^3. \tag{2.93}$$

Here, we have introduced the chemical potentials of all components into (2.89) and (2.90). The

[7] Note that for reactions in which components participate in both directions of the reaction, e.g. reaction (2.71), the present notation would need to be amended by introducing separate stochiometric coefficients for the forward and backward directions. Here, we stick to the notation used in [SP84] and instead interpret the prefactors appearing in front of the reactive fluxes J_j in Eqs. (2.83)-(2.88) as the stochiometric difference between both reaction directions when needed. In particular, this is the case for reaction (2.71). For example, the coefficient of component 1 is then 1 since in the forward direction, two parts are consumed and three parts are produced.

constants appearing in (2.92) and (2.93) are given by

$$k_1^f = k_1 \exp\left[\frac{\bar{\mu}_3^0}{k_b T}\right], \tag{2.94}$$

$$k_1^b = k_1 \exp\left[\frac{\zeta_1}{k_b T}\right], \tag{2.95}$$

$$k_2^f = k_2 \exp\left[\frac{\bar{\mu}_4^0 + \zeta_1}{k_b T}\right], \tag{2.96}$$

$$k_2^b = k_2 \exp\left[\frac{\bar{\mu}_5^0 + \zeta_2}{k_b T}\right], \tag{2.97}$$

$$k_3^f = k_3 \exp\left[\frac{2\zeta_1 + \zeta_2}{k_b T}\right], \tag{2.98}$$

$$k_3^b = k_3 \exp\left[\frac{3\zeta_1}{k_b T}\right], \tag{2.99}$$

$$k_4^f = k_4 \exp\left[\frac{\zeta_1}{k_b T}\right], \tag{2.100}$$

$$k_4^b = k_4 \exp\left[\frac{\bar{\mu}_6^0}{k_b T}\right], \tag{2.101}$$

$$D_{1,2} = k_b T \tilde{D}_{1,2}. \tag{2.102}$$

Finally, suppressing back reactions ($k_j^b = 0$) yields the Brusselator equations

$$\frac{\partial n_1}{\partial t} = D_1 \Delta n_1 + k_1^f - k_2^f n_1 + k_3^f n_1^2 n_2 - k_4^f n_1, \tag{2.103}$$

$$\frac{\partial n_2}{\partial t} = D_2 \Delta n_2 + k_2^f n_1 - k_3^f n_1^2 n_2. \tag{2.104}$$

Note that the suppression of back reactions breaks detailed balance independently of chemostatting.

3. Reactive Surfactants on Thin Films of Liquid

While chemical reactions are a valuable subject of study on their own, particularly interesting phenomena may be observed when they are part of more complex dynamics. For instance, the dynamics of some liquid covered by insoluble surfactants may be enriched by (driven) chemical reactions taking place between different species of surfactant. For the correct description of situations of this kind, it is generally insufficient to simply couple reactive dynamics to surface tension and wetting effects of the liquid in an ad hoc manner as interesting and important cross-coupling effects are then neglected and the model may be rendered thermodynamically inconsistent. Instead, it seems appropriate to assign an underlying energy functional which accounts for all energetic contributions. In accordance with (linear) thermodynamics and in the context of a gradient dynamics approach, the dynamics is then determined by variations of the energy functional with respect to the dynamical fields as well as the corresponding mobility matrices (Onsager matrices). Finally, this gradient structure can then be broken by introducing some external driving. In chapter 2, this gradient dynamics approach was extended to chemical reactions, in which the functional variations now enter the dynamical equations in a nonlinear manner. In the following, we give a thermodynamically consistent description of thin films of liquid covered by reactive, insoluble surfactants as an application of the results from chapter 2.

3.1 Equilibrium Drops Covered by Reactive, Insoluble Surfactants

It is known that the presence of surfactants locally alters the surface tension of a liquid and also changes its wetting properties. Macroscopically, the equilibrium contact angle θ_e of a liquid droplet resting on a flat, solid substrate is given by Young's law [You05]

$$\gamma \cos\theta_e + \gamma_{sl} - \gamma_{sg} = 0, \tag{3.1}$$

where γ is the surface tension of the liquid and γ_{sl} and γ_{sg} are the interfacial tensions associated with the solid-liquid and the solid-gas interface, respectively. On the mesoscopic scale, wettability is modeled by a wetting energy $f(h)$, where h is the height of the liquid film. From equilibrium considerations, it can be shown [GBQ04] that macro- and mesoscale descriptions are consistent if

$$f(h_a) = \gamma_{sg} - \gamma_{sl} - \gamma, \tag{3.2}$$

where h_a is the film height of the equilibrium adsorption layer surrounding the drop. This condition has been generalized to drops covered by an insoluble surfactant [Thi+18]. In the following, this result will be further generalized to drops covered by multiple, reactive surfactants.

3.2 Macroscopic Description

Consider a 2D liquid drop of radius R, covering a flat, solid substrate. The drop is covered by N different components of surfactant that may engage in chemical reactions. Each component of surfactant is identified with a particle density Γ_i (particles per unit interface area) and a mass per particle m_i, respectively. The dynamics must conserve the drop volume V and the

total mass of surfactant M, i.e.

$$V = \int_0^R h \,\mathrm{d}x, \tag{3.3}$$

$$M = \sum_{i=1}^{N} \left(\int_0^R \xi m_i \Gamma_i \,\mathrm{d}x + \int_R^\infty m_i \Gamma_i \,\mathrm{d}x \right), \tag{3.4}$$

where h is the local drop film height and $\xi = \sqrt{1 + (\partial_x h)^2}$ is the metric factor of the drop surface. The free energy functional of the system is given by[1]

$$\begin{aligned} \mathcal{F}[h, \mathbf{\Gamma}] = \int_0^R \left[\xi g(\mathbf{\Gamma}) + \gamma_{sl} - ph\right] \,\mathrm{d}x + \int_R^\infty g_{sg}(\mathbf{\Gamma}) \,\mathrm{d}x - \lambda_\Gamma \sum_{i=1}^{N} \left(\int_0^R \xi m_i \Gamma_i \,\mathrm{d}x \right. \\ \left. + \int_R^\infty m_i \Gamma_i \,\mathrm{d}x \right) + \lambda_h h(R), \end{aligned} \tag{3.5}$$

where γ_{sl} is the interfacial tension of the solid-liquid interface and g and g_{sg} are the free energy densities associated with the liquid-gas and solid-gas interfaces. For brevity, the surfactant densities Γ_i are collected in the field $\mathbf{\Gamma} = (\Gamma_1, \Gamma_2, \ldots, \Gamma_N)$. Additionally, the energy functional is supplemented by the Lagrange multipliers p and λ_Γ, expressing the conservation laws (3.3) and (3.4), respectively.[2] The Lagrange multiplier λ_h is connected to the geometric constraint that the film height must vanish at the drop radius, i.e.

$$\int_0^\infty \delta(x - R) h(x) \,\mathrm{d}x = h(R) = 0. \tag{3.6}$$

At equilibrium, the free energy is minimal and each variation of $\mathcal{F}$ must vanish separately. Varying $\Gamma_j(x)$ gives

$$\delta\mathcal{F} = \int_0^R \xi \left[\partial_{\Gamma_j} g - \lambda_\Gamma m_j\right] \delta\Gamma_j \,\mathrm{d}x + \int_R^\infty \left[\partial_{\Gamma_j} g_{sg} - \lambda_\Gamma m_j\right] \delta\Gamma_j \,\mathrm{d}x, \tag{3.7}$$

so that we obtain the equilibrium conditions

$$\partial_{\Gamma_j} g = \lambda_\Gamma m_j, \quad \text{for } x \in [0, R], \tag{3.8}$$

$$\partial_{\Gamma_j} g_{sg} = \lambda_\Gamma m_j, \quad \text{for } x \in (R, \infty). \tag{3.9}$$

At equilibrium, the chemical potential $\bar{\mu}_j$ of each component j of surfactant is thus given by $\lambda_\Gamma m_j$. We now assume that no phase separation can take place. In particular, this means that the systems of equations given by (3.8) and (3.9) have the *unique* solutions $\mathbf{\Gamma}_d = (\Gamma_{1,d}, \Gamma_{2,d}, \ldots, \Gamma_{N,d})$ and $\mathbf{\Gamma}_a = (\Gamma_{1,a}, \Gamma_{2,a}, \ldots, \Gamma_{N,a})$, respectively. It then follows that at equilibrium, Γ_j is constant on and away from the drop with

$$\Gamma_j = \Gamma_{j,d}, \quad \text{for } x \in [0, R], \tag{3.10}$$

$$\Gamma_j = \Gamma_{j,a}, \quad \text{for } x \in (R, \infty). \tag{3.11}$$

Finally, (3.8) and (3.9) then also result in

$$\partial_{\Gamma_j} g(\mathbf{\Gamma}_d) = \partial_{\Gamma_j} g_{sg}(\mathbf{\Gamma}_a). \tag{3.12}$$

[1] For symmetry reasons, only half the system is considered.

[2] In the present consideration, we assume that only the total mass of surfactant is conserved and that due to chemical reactions, all components may be converted into each another. If the underlying dynamics exhibits stricter conservation laws for the individual species, e.g., such that some subset of components is conserved separately, then this must be accounted for in the constraints of the minimization problem. As long as total mass is conserved, however, this will not change the following results but does alter the equilibrium solutions $h(x)$ and $\mathbf{\Gamma}(x)$, which are not computed explicitly here.

Next, varying $h(x)$ yields

$$\delta\mathcal{F} = \int_0^R \left[\frac{g - \lambda_\Gamma \sum_{i=1}^N m_i\Gamma_i}{\xi}\partial_x h\delta(\partial_x h) - p\delta h\right] \mathrm{d}x + \lambda_h \delta h(R) \tag{3.13}$$

$$= \left[\frac{g - \lambda_\Gamma \sum_{i=1}^N m_i\Gamma_i}{\xi}\partial_x h\delta h\right]_0^R - \int_0^R \left[\partial_x\left(\frac{g - \lambda_\Gamma \sum_{i=1}^N m_i\Gamma_i}{\xi}\partial_x h\right) + p\right]\delta h \,\mathrm{d}x + \lambda_h\delta h(R) \tag{3.14}$$

$$= \left[\lambda_h + \frac{g - \lambda_\Gamma \sum_{i=1}^N m_i\Gamma_i}{\xi}\partial_x h(R)\right]\delta h(R) - \int_0^R \left[\frac{g - \lambda_\Gamma \sum_{i=1}^N m_i\Gamma_i}{\xi^3}\partial_{xx} h + p\right]\delta h \,\mathrm{d}x. \tag{3.15}$$

Here, we used partial integration from Eq. (3.13) to (3.14). From Eq. (3.14) to (3.15), it was used that due to symmetry $\partial_x h(0) = 0$ and that at equilibrium, $\mathbf{\Gamma}_d$ and $g(\mathbf{\Gamma}_d)$ are independent of x. From varying $h(x)$ we thus obtain the conditions

$$\lambda_h = -\gamma\frac{\partial_x h}{\xi}, \quad \text{at } x = R, \tag{3.16}$$

$$p = -\gamma\kappa, \quad \text{for } x \in [0, R]\,, \tag{3.17}$$

where $\gamma = g - \sum_i(\partial_{\Gamma_i} g)\Gamma_i$ and $\kappa = \partial_{xx} h/\xi^3$ are identified as the surface tension and the curvature, respectively. Note that in this definition of γ, Eq. (3.8) has already been used to replace λ_Γ. It is now apparent that the Lagrange multiplier p corresponds to the system pressure at equilibrium. Lastly, varying R and evaluating the resulting expression for $x \to R$ gives (with $h(R) = 0$):

$$\delta\mathcal{F} = \left[\xi g(\mathbf{\Gamma}_d) + \gamma_{sl} - g_{sg}(\mathbf{\Gamma}_a) - \lambda_\Gamma\left(\xi\sum_{i=1}^N m_i\Gamma_{i,d} - \sum_{i=1}^N m_i\Gamma_{i,a}\right) + \lambda_h\partial_x h(R)\right]\delta R. \tag{3.18}$$

This results in the equilibrium condition

$$0 = \xi\gamma(\mathbf{\Gamma}_d) + \gamma_{sl} - \gamma_{sg}(\mathbf{\Gamma}_a) - \gamma\frac{(\partial_x h)^2}{\xi} = \frac{\gamma(\mathbf{\Gamma}_d)}{\xi} + \gamma_{sl} - \gamma_{sg}(\mathbf{\Gamma}_a), \tag{3.19}$$

where we have used the definitions for λ_h, γ and the interfacial tension $\gamma_{sg} = g_{sg} - \sum_i(\partial_{\Gamma_i} g_{sg})\Gamma_i$. Using $\xi^{-1} = \cos\theta_e$ for $x \to R$, since then $\partial_x h(R) = \tan\theta_e$, we finally obtain

$$0 = \gamma(\mathbf{\Gamma}_d)\cos\theta_e + \gamma_{sl} - \gamma_{sg}(\mathbf{\Gamma}_a). \tag{3.20}$$

This equation corresponds to Young's law in the presence of insoluble and reactive surfactants, excluding phase separation. Note that the same relation holds if there are no chemical reactions between the surfactant species. However, the equilibrium densities $\mathbf{\Gamma}_d$ and $\mathbf{\Gamma}_a$ will differ depending on whether chemical reactions may take place. For instance, if no reaction takes place all surfactant species are conserved separately, resulting in more minimization constraints with distinct Lagrange-multipliers. This may in turn lead to different values of the chemical potentials and thus to different surfactant densities on and away from the drop.

3.3 Mesoscopic Description

In analogy to the previous calculations, equilibrium conditions can also be derived in a mesoscopic setting. Here, the interactions between the solid substrate and the liquid are represented by a wetting potential $f(h, \mathbf{\Gamma})$ which approaches zero as $h \to \infty$. In general, f may also be dependent on the local surfactant densities. However, this dependence is subject to thermodynamic constraints due to a necessary consistency between macroscopic and mesoscopic models,

as we now show. As in the macroscopic consideration, the system is assigned a free energy functional

$$\mathcal{F} = \int_0^\infty \left[\gamma_{sl} + f(h, \mathbf{\Gamma}) + \xi g(h, \mathbf{\Gamma}) - ph - \lambda_\Gamma \sum_{i=1}^N \xi m_i \Gamma_i \right] \mathrm{d}x, \tag{3.21}$$

where due to symmetry again only half the system is considered. Similarly, the Lagrange multipliers p and λ_Γ again correspond to volume conservation of liquid and conservation of total surfactant mass. Note that the interfacial energy of surfactant $g(h, \mathbf{\Gamma})$ may now be film height dependent. This accounts for possible (attractive) interactions between the surfactant components on the drop surface and the solid substrate. From consistency with macroscopics, it follows that this dependence must vanish for large film heights, i.e., $\partial_h g \to 0$ for $h \to \infty$. In mesoscopic equilibrium, the substrate is covered by a thin adsorption layer of film height h_a away from the drop. It will be seen that this characteristic film height is determined collectively by f and g. The equilibrium conditions can again be derived by minimizing $\mathcal{F}$ with respect to $h(x)$ and $\mathbf{\Gamma}(x)$. This gives

$$p = \partial_h f + \xi \partial_h g - \partial_x \left[\left(g - \lambda_\Gamma \sum_{i=1}^N m_i \Gamma_i \right) \frac{\partial_x h}{\xi} \right], \tag{3.22}$$

$$\lambda_\Gamma m_j = \frac{\partial_{\Gamma_j} f}{\xi} + \partial_{\Gamma_j} g, \tag{3.23}$$

varying h and Γ_j, respectively. Eqs. (3.22) and (3.23) correspond to the Euler-Lagrange equations of the variational problem. Additionally, given a Langrangian $\mathcal{L}$ and a corresponding action functional

$$S[\boldsymbol{y}] = \int \mathrm{d}x \, \mathcal{L}(\boldsymbol{y}, \boldsymbol{y}') \tag{3.24}$$

with the functions $\boldsymbol{y} = (y_1(x), y_2(x), \ldots, y_N(x))$ and their derivatives $\boldsymbol{y}' = (y_1'(x), y_2'(x), \ldots, y_N'(x))$, the solutions to the corresponding variational problem can also be assigned a first integral

$$E = \mathcal{L} - \sum_{i=1}^N y_i' \frac{\partial \mathcal{L}}{\partial y_i'}, \tag{3.25}$$

where E is some constant. Since the integrand of (3.21) is only a function of $h, \partial_x h$ and $\mathbf{\Gamma}$, the associated first integral takes the form

$$E = \gamma_{sl} + f + \xi \left(g - \lambda_\Gamma \sum_{i=1}^N m_i \Gamma_i \right) - ph - \left(g - \lambda_\Gamma \sum_{i=1}^N m_i \Gamma_i \right) \frac{(\partial_x h)^2}{\xi} \tag{3.26}$$

$$= \gamma_{sl} + f - ph + \frac{g - \lambda_\Gamma \sum_{i=1}^N m_i \Gamma_i}{\xi}. \tag{3.27}$$

Expressions (3.22), (3.23) and (3.27) will now be compared in two different spatial regions of the equilibrium state, namely the adsorption layer and a wedge region with a constant slope $\tan\theta_e$ far away from the adsorption layer. The adsorption layer is characterized by a constant film height $h \to h_a$ so that $\partial_x h \to 0$ and $\xi \to 1$. In the wedge region, all mesoscopic quantities vanish, i.e., $f, \partial_h f, \partial_h g \to 0$ and the film-curvature vanishes so that $\partial_{xx} h \to 0$ and $\xi^{-1} = \cos\theta_e$. Equating the right hand sides of (3.22), (3.23) and (3.27) in both regions yields

$$\partial_h f\left(h_a, \mathbf{\Gamma}_a(x)\right) + \partial_h g\left(h_a, \mathbf{\Gamma}_a(x)\right) = \left[-\partial_x \left(g(\mathbf{\Gamma}_w(x)) - \lambda_\Gamma \sum_{i=1}^N m_i \Gamma_{i,w}(x) \right) \right] \frac{\partial_x h}{\xi}, \tag{3.28}$$

$$\partial_{\Gamma_j} f\left(h_a, \mathbf{\Gamma}_a(x)\right) + \partial_{\Gamma_j} g\left(h_a, \mathbf{\Gamma}_a(x)\right) = \partial_{\Gamma_j} g(\mathbf{\Gamma}_w(x)), \tag{3.29}$$

$$f(h_a, \mathbf{\Gamma}_a(x)) - ph_a + g(h_a, \mathbf{\Gamma}_a(x)) - \lambda_\Gamma \sum_{i=1}^N m_i \Gamma_{i,a} = -ph(x) + \frac{g(\mathbf{\Gamma}_w(x)) - \lambda_\Gamma \sum_{i=1}^N m_i \Gamma_{i,w}(x)}{\xi}. \tag{3.30}$$

Here, the left hand side corresponds to the adsorption layer. Note that in the wedge region, g is only a function of the surfactant densities and not of the film height. Furthermore, evaluating Eq. (3.23) in the wedge region and in the adsorption layer implies that $\mathbf{\Gamma}_w = \text{const.}$ and $\mathbf{\Gamma}_a = \text{const.}$, where we assume again that the corresponding systems of equations have unique solutions so that no phase separation may take place. Equations (3.28) to (3.30) then read

$$\partial_h f\left(h_a, \mathbf{\Gamma}_a\right) + \partial_h g\left(h_a, \mathbf{\Gamma}_a\right) = 0, \tag{3.31}$$

$$\partial_{\Gamma_j} f\left(h_a, \mathbf{\Gamma}_a\right) + \partial_{\Gamma_j} g\left(h_a, \mathbf{\Gamma}_a\right) = \partial_{\Gamma_j} g(\mathbf{\Gamma}_w), \tag{3.32}$$

$$f(h_a, \mathbf{\Gamma}_a) + g(h_a, \mathbf{\Gamma}_a) - \lambda_\Gamma \sum_{i=1}^{N} m_i \Gamma_{i,a} = \frac{g(\mathbf{\Gamma}_w) - \lambda_\Gamma \sum_{i=1}^{N} m_i \Gamma_{i,w}}{\xi}, \tag{3.33}$$

where in (3.33) we used that from evaluating (3.22) in the wedge region, it now follows that $p = 0$. With the help of (3.23) and $\xi^{-1} = \cos\theta_e$ in the wedge region, Eq. (3.33) can also be re-written as

$$f(h_a, \mathbf{\Gamma}_a) - \sum_{i=1}^{N} \Gamma_{i,a} \partial_{\Gamma_i} f(h_a, \mathbf{\Gamma}_a) + \gamma(h_a, \mathbf{\Gamma}_a) = \gamma(\mathbf{\Gamma}_w) \cos\theta_e, \tag{3.34}$$

where the definition of the surface tension $\gamma = g - \sum_{i=1}^{N} \Gamma_i \partial_{\Gamma_i} g$ has been used. Note that in the wedge region, γ is only a function of the surfactant densities, while in the adsorption layer the surface tension may be film height dependent. Equations (3.31), (3.32) and (3.34) allow one to determine the binodals of wedge-adsorption layer coexistence in terms of $h_a, \mathbf{\Gamma}_a, \mathbf{\Gamma}_w$ and θ_e if $f(h, \mathbf{\Gamma})$ and $g(h, \mathbf{\Gamma})$ are specified. In practice, it may be convenient to pick $\mathbf{\Gamma}_a$ as a control parameter and use Eqs. (3.31), (3.32) and (3.34) to first determine h_a, then $\mathbf{\Gamma}_w$ and finally θ_e.

3.4 Consistency between Macroscopic and Mesoscopic Approach

Equation (3.34) corresponds to a generalized mesoscopic Young's law in the presence of reactive, insoluble surfactants. Equations (3.31) and (3.32) provide the adsorption layer height and the relation between $\mathbf{\Gamma}_a$ and $\mathbf{\Gamma}_w$. Because (3.23) is film height invariant for macroscopic film heights ($h \gg h_a$), it can be seen that $\mathbf{\Gamma}_w$ is constant across the macroscopic part of the drop. This allows the association $\mathbf{\Gamma}_w = \mathbf{\Gamma}_d$ so that the macroscopic Young's law (3.20) and its mesoscopic counterpart (3.34) may be compared, which implies

$$f(h_a, \mathbf{\Gamma}_a) - \sum_{i=1}^{N} \Gamma_{i,a} \partial_{\Gamma_i} f(h_a, \mathbf{\Gamma}_a) = \gamma_{sg}(\mathbf{\Gamma}_a) - \gamma_{sl} - \gamma(h_a, \mathbf{\Gamma}_a). \tag{3.35}$$

Identifying $\mathbf{\Gamma}_w = \mathbf{\Gamma}_d$ also implies

$$\partial_{\Gamma_j} f\left(h_a, \mathbf{\Gamma}_a\right) + \partial_{\Gamma_j} g\left(h_a, \mathbf{\Gamma}_a\right) = \partial_{\Gamma_j} g_{sg}(\mathbf{\Gamma}_a) \tag{3.36}$$

due to Eqs. (3.12) and (3.32). Then, introducing (3.36) into (3.35) finally gives the consistency condition

$$f(h_a, \mathbf{\Gamma}_a) = g_{sg}(\mathbf{\Gamma}_a) - \gamma_{sl} - g(h_a, \mathbf{\Gamma}_a) \tag{3.37}$$

between the macroscopic and mesoscopic approaches.

Example: Application for Simple Surfactant Energies

Equation (3.37) can be used to determine the particular surfactant-dependence of the wetting energy for a given functional shape. Here, we choose a simple product ansatz

$$f(h, \mathbf{\Gamma}) = \chi(\mathbf{\Gamma}) \hat{f}(h) \tag{3.38}$$

with $\chi(0) = 1$. The surface free energies g and g_{sg} are given by

$$g(\mathbf{\Gamma}) = \gamma^0 + k_b T \sum_{i=1}^{N} \Gamma_i \left[\ln(\Gamma_i a_i^2) - 1 \right], \tag{3.39}$$

$$g_{sg}(\mathbf{\Gamma}) = \gamma_{sg}^0 + k_b T \sum_{i=1}^{N} \Gamma_i \left[\ln(\Gamma_i a_{sg,i}^2) - 1 \right], \tag{3.40}$$

where a_i and $a_{sg,i}$ represent characteristic length scales of surfactant component i and γ^0 and γ_{sg}^0 denote the respective surface free energies in the absence of surfactant. Equation (3.37) then leads to the relation

$$\chi(\mathbf{\Gamma}_a)\hat{f}(h_a) = \gamma_{sg}^0 - \gamma_{sl} - \gamma^0 + k_b T \sum_{i=1}^{N} \Gamma_{i,a} \ln \delta_i = \hat{f}(h_a) + k_b T \sum_{i=1}^{N} \Gamma_{i,a} \ln \delta_i, \tag{3.41}$$

where we have used the definition $\delta_i = a_{sg,i}^2 / a_i^2$ and the relation $\gamma_{sg}^0 - \gamma_{sl} - \gamma^0 = \hat{f}(h_a)$ as a special case of (3.37). Since (3.41) must hold for arbitrary $\mathbf{\Gamma}_a$, the general expression

$$\chi(\mathbf{\Gamma}) = 1 + \frac{k_b T}{\hat{f}(h_a)} \sum_{i=1}^{N} \Gamma_i \ln \delta_i \tag{3.42}$$

follows. Note that if a film height dependent g is used (or if a different ansatz for f is chosen), the dependence of $h_a(\mathbf{\Gamma}_a)$ on the surfactant densities due to Eq. (3.31) must be taken into consideration and should be introduced into (3.41) before the general expression for χ is deduced. Additionally, it is mentioned that Eq. (3.37) does at least approximately allow for a wetting energy that is independent of surfactant, i.e. $f = f(h)$, even when g is film height dependent. For instance, by choosing

$$g(h, \mathbf{\Gamma}) = \gamma^0 + k_b T \sum_{i=1}^{N} \Gamma_i \left[\ln(\Gamma_i a_i^2) - 1 + \zeta_i(h) \right], \tag{3.43}$$

$$g_{sg}(\mathbf{\Gamma}) = \gamma_{sg}^0 + k_b T \sum_{i=1}^{N} \Gamma_i \left[\ln(\Gamma_i a_{sg,i}^2) - 1 + \zeta_i(h_a) \right], \tag{3.44}$$

where $\zeta_i(h)$ represents some general film height dependence of g, and by setting $a_i = a_{sg,i}$, Eq. (3.37) becomes

$$f(h_a, \mathbf{\Gamma}_a) = \gamma_{sg}^0 - \gamma_{sl} - \gamma^0, \tag{3.45}$$

$$\Rightarrow f(h_a, \mathbf{\Gamma}_a) = f(h_a). \tag{3.46}$$

From (3.45) to (3.46), we have assumed that h_a does not change too drastically with $\mathbf{\Gamma}_a$ due to Eq. (3.31) and is consequently treated as a constant. Then, f can be seen as a function of h only as the right hand side of (3.45) is constant and (3.45) must hold for arbitrary $\mathbf{\Gamma}_a$. Thus, the contributions of surfactant densities to the pressure p stem only from the film height dependence of the surface free energy $g(h, \mathbf{\Gamma})$.

3.5 Dynamical Equations

Following the equilibrium considerations of Sec. 3.1, one can now choose an energy functional with thermodynamically consistent contributions that can be employed in a gradient dynamics structure to obtain dynamical equations for a thin film of liquid covered by N reactive surfactants. In this case, the generic shape of the free energy functional is given by

$$\mathcal{F} = \int_\Omega \left[f(h, \mathbf{\Gamma}) + \xi g(h, \mathbf{\Gamma}) \right] \mathrm{d}^2 x, \tag{3.47}$$

where $\xi = \sqrt{1+(\nabla h)^2}$ is the metric-factor with $\nabla = (\partial_x, \partial_y)^{\mathrm{T}}$ and Ω denotes the two-dimensional spatial domain. Note that the constant solid-liquid interfacial tension γ_{sl} was omitted. The wetting energy f and the surface free energy g must obey the consistency conditions derived in Sec. 3.1. Before a gradient dynamics formulation of the dynamical equations can be given, we must first determine the correct dynamical fields with respect to which the (free) energy functional must be varied. As it will turn out, these fields are *not* the film height h and the surface density of surfactants $\mathbf{\Gamma} = (\Gamma_1, \Gamma_2)$ but rather the film height and the "projected" densities $\tilde{\mathbf{\Gamma}} = \xi\mathbf{\Gamma}$. To show this, we observe that thermodynamically, the functional derivatives of the associated energy functional must correspond to thermodynamic quantities such as the pressure or chemical potentials. In the usual thin-film geometry, a liquid film moves on a flat substrate that is not subject to any dynamics. Consider now a vertical column of base area $\mathrm{d}A$ at the substrate and of film height h. The liquid volume $\mathrm{d}V$ and the particle count $\mathrm{d}N_i$ of component i of surfactant in this column are then given by

$$\mathrm{d}V = h\mathrm{d}A, \tag{3.48}$$

$$\mathrm{d}N_i = \Gamma_i \mathrm{d}S = \tilde{\Gamma}_i \mathrm{d}A, \tag{3.49}$$

where $\mathrm{d}S = \xi\mathrm{d}A$ is the film surface area in the column. Assuming local thermodynamic equilibrium, the pressure p and the chemical potential $\bar{\mu}_i$ are obtained as derivatives of the free energy F in the column:

$$p = \left(\frac{\partial F}{\partial V}\right)_{T,V,N_1,\ldots,N_N}, \tag{3.50}$$

$$\bar{\mu}_i = \left(\frac{\partial F}{\partial N_i}\right)_{T,V,N_{j\neq i}}. \tag{3.51}$$

Here, the subscripts denote quantities that are kept constant during differentiation. It is now crucial to observe that when changing $\mathrm{d}V$ by varying the film height profile h ($\mathrm{d}A$ is constant in the present geometry) and keeping Γ_i constant, then the particle count $\mathrm{d}N_i$ *does change* since $\mathrm{d}S$ depends on the film height profile. Therefore, while varying h does directly correspond to only altering the volume in the column, the surface density Γ_i does not directly translate to a change in only $\mathrm{d}N_i$. Thus, variations of the free energy with respect to h and Γ_i do not yield the correct pressure and chemical potentials as the thermodynamic constraints for differentiation are not met. Changes in the projected density $\tilde{\Gamma}_i$, however, do directly coincide with a change in only $\mathrm{d}N_i$, since $\mathrm{d}A$ is constant. For this reason, to calculate the pressure p and the chemical potential, the free energy functional (3.47) has to be varied with respect to h and $\tilde{\Gamma}_i$ as changes in these fields are equivalent to changes in volume or particle count in the thin-film geometry.[3] Thus, the pressure and the chemical potentials can be written as[4]

$$p = \frac{\delta\mathcal{F}}{\delta h}, \tag{3.52}$$

$$\bar{\mu}_i = \frac{\delta\mathcal{F}}{\delta\tilde{\Gamma}_i}. \tag{3.53}$$

Having found the correct dynamical fields and the related pressure and chemical potentials, the dynamical equations can now be obtained by combining the usual approach of linear thermodynamics for transport processes, such as advection and diffusion, with the previously discussed

[3] Note that this is not necessary for the minimization procedure carried out in Secs. 3.2 and 3.3 because the pressure and chemical potentials are not computed explicitly by varying the free energy functional but are obtained as Lagrange multipliers. Since it is irrelevant whether the free energy minimum is expressed in terms of $(h, \mathbf{\Gamma})$ or $(h, \tilde{\mathbf{\Gamma}})$, one obtains the correct Lagrange multipliers in any case.

[4] This is because the free energy *functional* (3.47) is obtained by integrating over the substrate coordinates so that taking its functional derivative with respect to h or $\tilde{\Gamma}_i$ translates to differentiating a (local) free energy *function* with respect to $h\mathrm{d}A$ or $\tilde{\Gamma}_i\mathrm{d}A$. These quantities then directly correspond to the volume and the particle count at a particular point in substrate coordinates, as we have discussed before.

reactive fluxes that are nonlinear in the energy variations. For example, for a thin film covered by two species of insoluble surfactant Γ_1 and Γ_2 that can engage in a conversion reaction

$$\Gamma_1 \leftrightharpoons \Gamma_2, \tag{3.54}$$

the dynamical equations are then given by

$$\partial_t h = \nabla \cdot \left[Q_{hh} \nabla \frac{\delta \mathcal{F}}{\delta h} + Q_{h\Gamma_1} \nabla \frac{\delta \mathcal{F}}{\delta \tilde{\Gamma}_1} + Q_{h\Gamma_2} \nabla \frac{\delta \mathcal{F}}{\delta \tilde{\Gamma}_2} \right], \tag{3.55}$$

$$\partial_t \tilde{\Gamma}_1 = \nabla \cdot \left[Q_{\Gamma_1 h} \nabla \frac{\delta \mathcal{F}}{\delta h} + Q_{\Gamma_1 \Gamma_1} \nabla \frac{\delta \mathcal{F}}{\delta \tilde{\Gamma}_1} + Q_{\Gamma_1 \Gamma_2} \nabla \frac{\delta \mathcal{F}}{\delta \tilde{\Gamma}_2} \right] + k \left[\exp\left(\frac{1}{k_b T} \frac{\delta \mathcal{F}}{\delta \tilde{\Gamma}_2} \right) - \exp\left(\frac{1}{k_b T} \frac{\delta \mathcal{F}}{\delta \tilde{\Gamma}_1} \right) \right], \tag{3.56}$$

$$\partial_t \tilde{\Gamma}_2 = \nabla \cdot \left[Q_{\Gamma_2 h} \nabla \frac{\delta \mathcal{F}}{\delta h} + Q_{\Gamma_2 \Gamma_1} \nabla \frac{\delta \mathcal{F}}{\delta \tilde{\Gamma}_1} + Q_{\Gamma_2 \Gamma_2} \nabla \frac{\delta \mathcal{F}}{\delta \tilde{\Gamma}_2} \right] - k \left[\exp\left(\frac{1}{k_b T} \frac{\delta \mathcal{F}}{\delta \tilde{\Gamma}_2} \right) - \exp\left(\frac{1}{k_b T} \frac{\delta \mathcal{F}}{\delta \tilde{\Gamma}_1} \right) \right]. \tag{3.57}$$

Here, $k > 0$ denotes the rate of the conversion reaction. The mobility matrix $\underline{\boldsymbol{Q}}$ is given by

$$\underline{\boldsymbol{Q}} = \begin{pmatrix} \frac{h^3}{3\eta} & \frac{h^2 \Gamma_1}{2\eta} & \frac{h^2 \Gamma_2}{2\eta} \\ \frac{h^2 \Gamma_1}{2\eta} & \frac{h \Gamma_1^2}{\eta} + M_1(\Gamma_1) & \frac{h \Gamma_1 \Gamma_2}{\eta} \\ \frac{h^2 \Gamma_2}{2\eta} & \frac{h \Gamma_1 \Gamma_2}{\eta} & \frac{h \Gamma_2^2}{\eta} + M_2(\Gamma_2) \end{pmatrix}, \tag{3.58}$$

where η is the dynamic viscosity of the liquid and $M_{1,2}$ are positive diffusive mobilities.[5] For thin films covered by a single species of surfactant, a gradient dynamics formulation has already been given [TAP12; TAP16]. The mobility matrix (3.58) is a generalization of this case. A derivation of dynamical equations containing multiple surfactant fields, from which (3.58) may be inferred, can be found in [Per+07]. Note that (3.58) is symmetric and positive (semi-)definite, accounting for microscopic reversibility and non-negative entropy production[6]. In analogy to the calculation (2.46)-(2.50) presented in Sec. 2.3, it can therefore be shown that $\mathcal{F}$ decreases monotonically with time and is a Lyapunov-functional to the dynamics (3.55)-(3.57). For the free energy functional (3.47), now expressed as a functional of h and $\tilde{\boldsymbol{\Gamma}}$

$$\mathcal{F}[h, \tilde{\boldsymbol{\Gamma}}] = \int_\Omega \left[f(h, \tfrac{\tilde{\boldsymbol{\Gamma}}}{\xi}) + \xi g(h, \tfrac{\tilde{\boldsymbol{\Gamma}}}{\xi}) \right] \mathrm{d}^2 x, \tag{3.59}$$

the corresponding variations are given by

$$p = \frac{\delta \mathcal{F}}{\delta h} = \partial_h f + \xi \partial_h g - \nabla \cdot \left[\tfrac{1}{\xi} \left(g - \sum_{i=1}^{N} \Gamma_i \partial_{\Gamma_i} g + \tfrac{\Gamma_i}{\xi} \partial_{\Gamma_i} f \right) \nabla h \right], \tag{3.60}$$

$$\bar{\mu}_i = \frac{\delta \mathcal{F}}{\delta \tilde{\Gamma}_i} = \partial_{\Gamma_i} g + \tfrac{1}{\xi} \partial_{\Gamma_i} f. \tag{3.61}$$

[5] Note that because it is assumed that the film surface is only sparsely covered by surfactant, the diffusive mobilities can be chosen independently, since other components covering the surface are not part of the model.

[6] Note that (3.58) is only semi-definite if diffusion is not considered. In time simulations, this leads to steady states with non-vanishing chemical potential gradients. If the chemical potential gradients were still thermodynamic forces in the absence of diffusion, then the thermodynamic equilibrium conditions would be violated. Here, further work is required.

Introducing these variations into the dynamical equations (3.55)-(3.57), we then obtain in the long-wave limit $\xi \approx 1$

$$\begin{aligned}\partial_t h = \nabla \cdot [&Q_{hh}\nabla\{\partial_h f + \partial_h g - \nabla \cdot [(g - \textstyle\sum_{i=1}^{2} \Gamma_i \partial_{\Gamma_i} g + \Gamma_i \partial_{\Gamma_i} f)\nabla h]\} \\ &+ Q_{h\Gamma_1}\nabla\{\partial_{\Gamma_1} g + \partial_{\Gamma_1} f\} + Q_{h\Gamma_2}\nabla\{\partial_{\Gamma_2} g + \partial_{\Gamma_2} f\}],\end{aligned} \tag{3.62}$$

$$\begin{aligned}\partial_t \Gamma_1 = \nabla \cdot [&Q_{\Gamma_1 h}\nabla\{\partial_h f + \partial_h g - \nabla \cdot [(g - \textstyle\sum_{i=1}^{2} \Gamma_i \partial_{\Gamma_i} g + \Gamma_i \partial_{\Gamma_i} f)\nabla h]\} \\ &+ Q_{\Gamma_1\Gamma_1}\nabla\{\partial_{\Gamma_1} g + \partial_{\Gamma_1} f\} + Q_{\Gamma_1\Gamma_2}\nabla\{\partial_{\Gamma_2} g + \partial_{\Gamma_2} f\}] \\ &+ k[\exp\{\tfrac{1}{k_b T}(\partial_{\Gamma_2} g + \partial_{\Gamma_2} f)\} - \exp\{\tfrac{1}{k_b T}(\partial_{\Gamma_1} g + \partial_{\Gamma_1} f)\}],\end{aligned} \tag{3.63}$$

$$\begin{aligned}\partial_t \Gamma_2 = \nabla \cdot [&Q_{\Gamma_2 h}\nabla\{\partial_h f + \partial_h g - \nabla \cdot [(g - \textstyle\sum_{i=1}^{2} \Gamma_i \partial_{\Gamma_i} g + \Gamma_i \partial_{\Gamma_i} f)\nabla h]\} \\ &+ Q_{\Gamma_2\Gamma_1}\nabla\{\partial_{\Gamma_1} g + \partial_{\Gamma_1} f\} + Q_{\Gamma_2\Gamma_2}\nabla\{\partial_{\Gamma_2} g + \partial_{\Gamma_2} f\}] \\ &+ k[\exp\{\tfrac{1}{k_b T}(\partial_{\Gamma_1} g + \partial_{\Gamma_1} f)\} - \exp\{\tfrac{1}{k_b T}(\partial_{\Gamma_2} g + \partial_{\Gamma_2} f)\}].\end{aligned} \tag{3.64}$$

Example: Film Height Dependent Suppression of Chemical Reactions

Equations (3.62)-(3.64) may now be supplemented by specific expressions for f and g to describe particular systems and effects. For instance, interactions between surfactants and the substrate play a key role in the formation of patterns by substrate-mediated condensation and during Langmuir-Blodgett transfer [Köp+10; Wil16]. These interactions may be incorporated into thin-film models by introducing either a surfactant dependence into the wetting energy f or by making the free surface energy g film height dependent. In the context of reactive surfactants, an interesting coupling in the reactive terms of (3.63) and (3.64) arises if g is chosen as

$$g(h, \Gamma_1, \Gamma_2) = \gamma^0 + k_b T\{\Gamma_1[\ln(\Gamma_1 a_1^2) - 1 + \zeta(h)] + \Gamma_2[\ln(\Gamma_2 a_2^2) - 1]\}, \tag{3.65}$$

where

$$\zeta(h) = \ln\left[\tfrac{1}{2}\left(1 + \tanh\left(\tfrac{h-h_0}{\Delta h}\right)\right)\right] \tag{3.66}$$

expresses attractive interactions between the substrate and surfactant component Γ_1 (see Fig. 3.1). Here, h_0 and Δh are positive constants. The partial derivatives of g are then given by

$$\partial_h g = k_b T \Gamma_1 \partial_h \zeta = \frac{k_b T \Gamma_1}{\Delta h} \frac{\operatorname{sech}^2\left(\tfrac{h-h_0}{\Delta h}\right)}{1 + \tanh\left(\tfrac{h-h_0}{\Delta h}\right)}, \tag{3.67}$$

$$\partial_{\Gamma_1} g = k_b T\left[\ln(\Gamma_1 a_1^2) + \zeta(h)\right], \tag{3.68}$$

$$\partial_{\Gamma_2} g = k_b T \ln(\Gamma_2 a_2^2). \tag{3.69}$$

Note that $\partial_h g$ is a step-like function with $\partial_h g \to 0$ for $h \to \infty$ (cf. $\partial_h \zeta$ in Fig. 3.1). Therefore, the corresponding pressure contribution vanishes for macroscopic film heights (if h_0 and Δh are mesoscopic quantities) and is a mesoscopic effect.

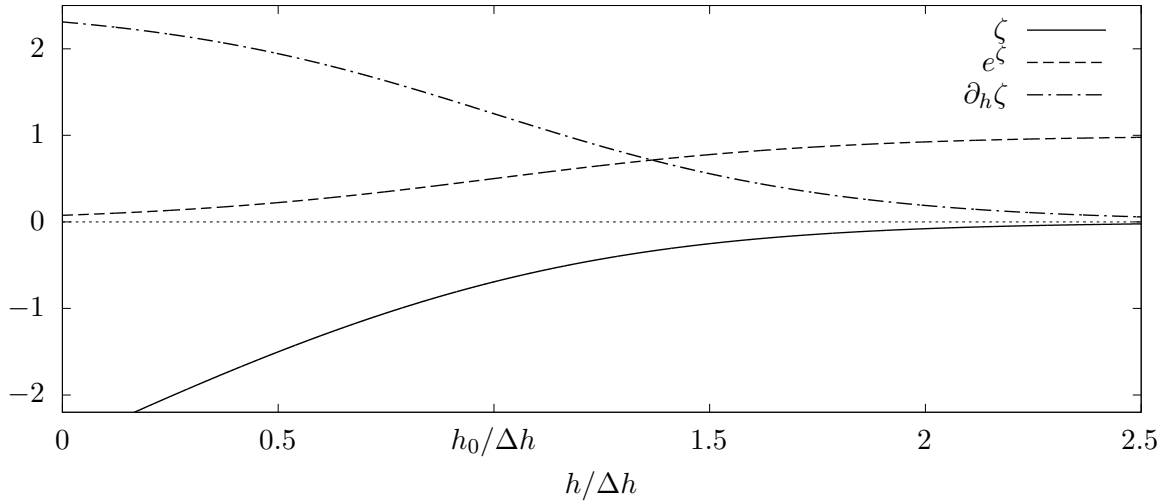

Figure 3.1: Expressions ζ, e^{ζ} and $\partial_h \zeta$ as functions of $h/\Delta h$ for $h_0/\Delta h = 1$. ζ expresses mesosocpic attractive interactions between surfactant component Γ_1 and the substrate, $\partial_h \zeta$ corresponds to the respective mesoscopic pressure contribution and e^{ζ} expresses the resulting film height dependent suppression of the conversion $\Gamma_1 \to \Gamma_2$. As a visual cue, a dotted baseline is drawn.

The reactive flux J appearing in (3.63) and (3.64) now reads

$$J = k \left[a_2^2 e^{\frac{1}{k_b T} \partial_{\Gamma_2} f} \Gamma_2 - \tfrac{1}{2} \left(1 + \tanh \left(\tfrac{h - h_0}{\Delta h} \right) \right) a_1^2 e^{\frac{1}{k_b T} \partial_{\Gamma_1} f} \Gamma_1 \right]. \tag{3.70}$$

Therefore, the conversion $\Gamma_1 \to \Gamma_2$ is suppressed for small film heights ($h < h_0$) due to the attractive interactions between the surfactant Γ_1 and the substrate (cf. e^{ζ} in Fig. 3.1). In some models, this kind of film height dependent suppression is made plausible by comparison with experiments [TJB04; JBT05]. Here, it is obtained from casting the dynamical equations into a thermodynamically consistent form based on a gradient dynamics approach.

4. Non-Equilibrium Drops with Autocatalysis and Evaporation

Phenomena related to reactive fluids are encountered on virtually every scale, ranging from convective motion in stars, to atmospheric chemistry, combustion in engines and turbines [De 20], the growth of biofilms [Tri18] and protein patterns within cells [Bur+22]. In particular, the interplay between autocatalytic chemical reactions, surface tension and the dynamics of drops is expected to have played a key role in the formation of the first cells [Zwi+17; Don+20; Ian+22]. In relation to some of these biological systems and in the context of chapter 3, in this chapter we study a model describing a thin film covered by surfactants with autocatalysis. The system is permanently driven out of equilibrium by evaporation and condensation of the surfactants. In Sec. 4.1, the general form of the model and its dynamical equations are presented. The linear stability of a flat film is then analyzed in Sec. 4.2. Finally, we study the rich fully non-linear behavior in Sec. 4.3 using a combination of numerical continuation and time simulations.

4.1 Model Equations

We consider a shallow drop of partially wetting liquid that is covered by two species of insoluble surfactants (Fig. 4.1) that may engage in the autocatalytic reaction

$$2\Gamma_1 + \Gamma_2 \rightleftharpoons 3\Gamma_1. \tag{4.1}$$

Here, $\Gamma_{1,2}$ denote the particle densities of the individual species (particles per unit interface area). Both species may also transition into the surrounding vapor phases (densities $\Gamma_{1,g}$ and $\Gamma_{2,g}$, particles per unit substrate area[1]).

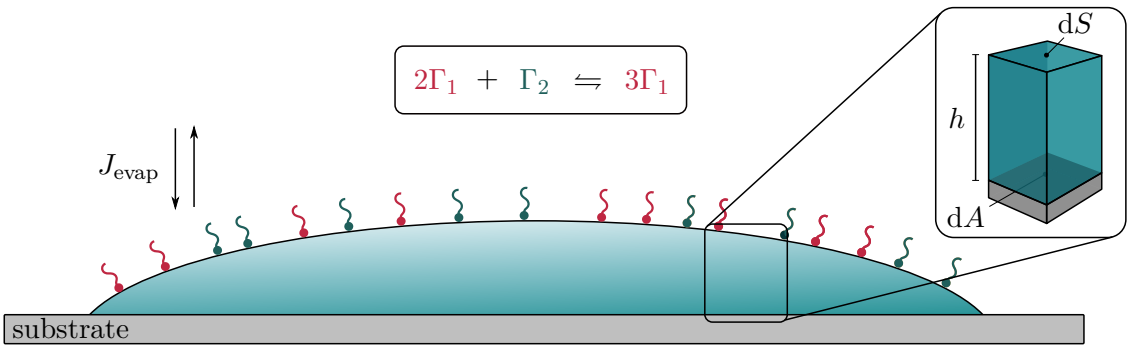

Figure 4.1: Sketch of the considered model system. A shallow drop of partially wetting liquid sits on a solid substrate and is covered by two species of surfactants. The surfactants engage in an autocatalytic reaction and an exchange with the vapor phase is possible by evaporation and condensation. The inset shows the typical thin-film geometry with the film height h and the substrate and surface areas $\mathrm{d}A$ and $\mathrm{d}S$, respectively.

The free energy of the system is given by

$$\mathcal{F} = \int_\Omega \left[f(h) + \xi g_s(\Gamma_1, \Gamma_2) + g_g(\Gamma_{1,g}, \Gamma_{2,g}) \right] \mathrm{d}^2x, \tag{4.2}$$

[1]Usually, bulk densities are given as particles per unit volume. Here, it is assumed that the vapor phases equilibrate fast in the vertical direction so that $\Gamma_{1,g}$ and $\Gamma_{2,g}$ represent some vertically integrated densities per unit area of substrate. Generally, the gas phase dynamics is treated rather crudely here since the vertical integration of the bulk densities leads to a film height dependence of the fields and the free energy and thus to a pressure contribution. Since the bulk densities will be assumed fixed in the following, this pressure contribution only amounts to a constant and can be neglected. For a gradient dynamics treatment of non-chemostatted gas phases in the thin film geometry, see [Har+23].

where $f(h)$ is the wetting energy, $g_s(\Gamma_1, \Gamma_2)$ is the surface free energy of surfactant and $g_g(\Gamma_{1,g}, \Gamma_{2,g})$ is the bulk free energy of the gaseous surfactant phases. A possible surfactant-dependence of the wetting energy is neglected. The corresponding pressure p and the chemical potentials on the surface $\bar{\mu}_i$ and in the gaseous phase $\bar{\mu}_{i,g}$ are given by

$$p = \frac{\delta \mathcal{F}}{\delta h} = \partial_h f - \nabla \cdot \left[\tfrac{1}{\xi} \left(g_s - \Gamma_1 \partial_{\Gamma_1} g_s - \Gamma_2 \partial_{\Gamma_2} g_s \right) \nabla h \right], \tag{4.3}$$

$$\bar{\mu}_i = \frac{\delta \mathcal{F}}{\delta \tilde{\Gamma}_i} = \partial_{\Gamma_i} g_s, \tag{4.4}$$

$$\bar{\mu}_{i,g} = \frac{\delta \mathcal{F}}{\delta \Gamma_{i,g}} = \partial_{\Gamma_{i,g}} g_g. \tag{4.5}$$

Here, $\tilde{\Gamma}_i = \xi \Gamma_i$ denotes the projected surfactant density. The dynamical equations are then given by[2]

$$\partial_t h = \nabla \cdot \left[Q_{hh} \nabla \frac{\delta \mathcal{F}}{\delta h} + Q_{h\Gamma_1} \nabla \frac{\delta \mathcal{F}}{\delta \tilde{\Gamma}_1} + Q_{h\Gamma_2} \nabla \frac{\delta \mathcal{F}}{\delta \tilde{\Gamma}_2} \right], \tag{4.6}$$

$$\partial_t \tilde{\Gamma}_1 = \nabla \cdot \left[Q_{\Gamma_1 h} \nabla \frac{\delta \mathcal{F}}{\delta h} + Q_{\Gamma_1 \Gamma_1} \nabla \frac{\delta \mathcal{F}}{\delta \tilde{\Gamma}_1} + Q_{\Gamma_1 \Gamma_2} \nabla \frac{\delta \mathcal{F}}{\delta \tilde{\Gamma}_2} \right] + J_r + J_{\text{evap},1}, \tag{4.7}$$

$$\partial_t \tilde{\Gamma}_2 = \nabla \cdot \left[Q_{\Gamma_2 h} \nabla \frac{\delta \mathcal{F}}{\delta h} + Q_{\Gamma_2 \Gamma_1} \nabla \frac{\delta \mathcal{F}}{\delta \tilde{\Gamma}_1} + Q_{\Gamma_2 \Gamma_2} \nabla \frac{\delta \mathcal{F}}{\delta \tilde{\Gamma}_2} \right] - J_r + J_{\text{evap},2}, \tag{4.8}$$

$$\partial_t \Gamma_{1,g} = -J_{\text{evap},1}, \tag{4.9}$$

$$\partial_t \Gamma_{2,g} = -J_{\text{evap},2}. \tag{4.10}$$

The mobility matrix $\underline{\boldsymbol{Q}}$ is given by

$$\underline{\boldsymbol{Q}} = \begin{pmatrix} \frac{h^3}{3\eta} & \frac{h^2 \Gamma_1}{2\eta} & \frac{h^2 \Gamma_2}{2\eta} \\ \frac{h^2 \Gamma_1}{2\eta} & \frac{h \Gamma_1^2}{\eta} + M_1(\Gamma_1) & \frac{h \Gamma_1 \Gamma_2}{\eta} \\ \frac{h^2 \Gamma_2}{2\eta} & \frac{h \Gamma_1 \Gamma_2}{\eta} & \frac{h \Gamma_2^2}{\eta} + M_2(\Gamma_2) \end{pmatrix}, \tag{4.11}$$

where η is the dynamic viscosity of the liquid and $M_{1,2}$ are positive diffusive mobilities. The reactive fluxes and the evaporation and condensation fluxes [FAT12] are given by

$$J_r = r \left[\exp\left(\frac{2}{k_b T} \frac{\delta \mathcal{F}}{\delta \tilde{\Gamma}_1} + \frac{1}{k_b T} \frac{\delta \mathcal{F}}{\delta \tilde{\Gamma}_2} \right) - \exp\left(\frac{3}{k_b T} \frac{\delta \mathcal{F}}{\delta \tilde{\Gamma}_1} \right) \right], \tag{4.12}$$

$$J_{\text{evap},i} = -\beta_i \left(\frac{\delta \mathcal{F}}{\delta \tilde{\Gamma}_i} - \frac{\delta \mathcal{F}}{\delta \Gamma_{i,g}} \right). \tag{4.13}$$

Here, $r > 0$ and $\beta_i > 0$ denote the reaction and evaporation rates, respectively. We now assume that the chemical potentials of the vapor phases are fixed ($\bar{\mu}_{i,g} = \text{const.}$), e.g., by the use of some chemostat or because the vapor phases are present in vast excess, so that the system is driven by evaporation and condensation. The time evolution of the gaseous phases is then given by

$$\partial_t \Gamma_{1,g} = -J_{\text{evap},1} + J_{C,1} = 0, \tag{4.14}$$

$$\partial_t \Gamma_{2,g} = -J_{\text{evap},2} + J_{C,2} = 0, \tag{4.15}$$

where $J_{C,i}$ represent the action of the external chemostat. The remaining dynamical equations can then be reduced to (4.6)-(4.8) with

$$J_{\text{evap},i} = -\beta_i \left(\frac{\delta \mathcal{F}}{\delta \tilde{\Gamma}_i} - \bar{\mu}_{i,g} \right). \tag{4.16}$$

[2] For simplicity, we only consider evaporation and condensation for the vapor phases, as the respective chemical potentials are kept constant in further considerations. For a complete description without subsequent chemostatting, convective transport and chemical reactions should be considered.

In the following, we only consider entropic contributions to the density-dependent part of the surface free energy, i.e.

$$g_s(\Gamma_1,\Gamma_2) = \gamma^0 + k_bT\Gamma_1[\ln(\Gamma_1 a_1^2) - 1] + k_bT\Gamma_2[\ln(\Gamma_2 a_2^2) - 1], \tag{4.17}$$

where $a_{1,2} > 0$ are characteristic length scales of the two surfactants and γ^0 is the surface tension in the absence of surfactant. The pressure and chemical potentials can now be specified as

$$p = \partial_h f - \nabla\cdot\left[\tfrac{1}{\xi}\left(\gamma^0 - k_bT\Gamma_1 - k_bT\Gamma_2\right)\nabla h\right], \tag{4.18}$$

$$\bar{\mu}_i = k_bT\ln(\Gamma_i a_i^2). \tag{4.19}$$

In addition, it will be assumed that $\xi \approx 1$ and that the changes in surface tension due to the presence of surfactant are small compared to γ^0. Then the pressure is given by

$$p = \partial_h f - \gamma^0\Delta h. \tag{4.20}$$

Furthermore, the driving forces associated with evaporation and condensation will always be of identical magnitude but different sign for further considerations, that is

$$-\beta_1\bar{\mu}_{1,g} = \beta_2\bar{\mu}_{2,g} \equiv \beta\mu \geq 0. \tag{4.21}$$

Therefore, evaporation of the reaction product Γ_1 is favored while the reactant Γ_2 tends to condense on the free surface. Note that for $\beta\mu = 0$ a passive system is recovered. Because the chemical potentials of the gaseous phases are then kept at zero, the respective particle counts may be freely manipulated without changing the local free energy of the system. Consequently, despite fixing the chemical potentials and thus the particle densities of the vapor phases there is no energy influx. Indeed, for $\beta\mu = 0$ equations (4.6)-(4.8) are again a three-field gradient dynamics. Therefore, by varying $\beta\mu$ the transition to an active system can be studied if the remaining parameters are fixed. In total, equations (4.6)-(4.8) simplify to

$$\partial_t h = \nabla\cdot\left[\frac{h^3}{3\eta}\nabla p\right] + k_bT\nabla\cdot\left[\frac{h^2}{2\eta}\nabla\Gamma_1\right] + k_bT\nabla\cdot\left[\frac{h^2}{2\eta}\nabla\Gamma_2\right], \tag{4.22}$$

$$\begin{aligned}\partial_t\Gamma_1 = {}& \nabla\cdot\left[\frac{h^2\Gamma_1}{2\eta}\nabla p\right] + k_bT\nabla\cdot\left[\left(\frac{h\Gamma_1}{\eta} + D_1\right)\nabla\Gamma_1\right] + k_bT\nabla\cdot\left[\frac{h\Gamma_1}{\eta}\nabla\Gamma_2\right] \\ & + r\left[\left(\Gamma_1 a_1^2\right)^2\left(\Gamma_2 a_2^2\right) - \left(\Gamma_1 a_1^2\right)^3\right] - \beta_1 k_bT\ln(\Gamma_1 a_1^2) - \beta\mu,\end{aligned} \tag{4.23}$$

$$\begin{aligned}\partial_t\Gamma_2 = {}& \nabla\cdot\left[\frac{h^2\Gamma_2}{2\eta}\nabla p\right] + k_bT\nabla\cdot\left[\frac{h\Gamma_2}{\eta}\nabla\Gamma_1\right] + k_bT\nabla\cdot\left[\left(\frac{h\Gamma_2}{\eta} + D_2\right)\nabla\Gamma_2\right] \\ & - r\left[\left(\Gamma_1 a_1^2\right)^2\left(\Gamma_2 a_2^2\right) - \left(\Gamma_1 a_1^2\right)^3\right] - \beta_2 k_bT\ln(\Gamma_2 a_2^2) + \beta\mu.\end{aligned} \tag{4.24}$$

Here, the mobilities $M_i = D_i\Gamma_i$ with the diffusion constants $D_i > 0$ were used.

Non-dimensionalization

For further analysis, we now bring the model (4.22)-(4.24) into a dimensionless form by introducing the scaling

$$t = \tau\tilde{t}, \qquad (x,y) = L(\tilde{x},\tilde{y}), \qquad h = l\tilde{h}, \qquad \Gamma_i = a_1a_2\tilde{\Gamma}_i \qquad (f,g_s) = \kappa(\tilde{f},\tilde{g}_s), \tag{4.25}$$

where dimensionless quantities are denoted by tildes. The respective scales are chosen as

$$\tau = \frac{L^2\eta}{\kappa l}, \qquad L = \sqrt{\frac{\gamma^0}{\kappa}}l, \qquad l = h_a, \qquad \kappa = \frac{k_bT}{a_1a_2}. \tag{4.26}$$

Here, h_a denotes the precursor film height, as determined by the wetting energy $f(h)$. In this case, the wetting energy is chosen as

$$f(h) = A\left(-\frac{1}{2h^2} + \frac{h_a^3}{5h^5}\right), \tag{4.27}$$

where A is the Hamaker constant. (4.27) corresponds to a partially wetting liquid. Note that for this particular choice of scales the long-wave approximation $L \gg l$ simplifies to $\gamma^0 \gg \frac{k_bT}{a_1a_2}$. Therefore, neglecting surfactant contributions to the capillary pressure is consistent with the present scaling. The non-dimensional equations are now given by

$$\partial_{\tilde{t}}\tilde{h} = \tilde{\nabla}\cdot\left[\frac{\tilde{h}^3}{3}\tilde{\nabla}\left[W\left(\frac{1}{\tilde{h}^3} - \frac{1}{\tilde{h}^6}\right) - \tilde{\Delta}\tilde{h}\right]\right] + \tilde{\nabla}\cdot\left[\frac{\tilde{h}^2}{2}\tilde{\nabla}\tilde{\Gamma}_1\right] + \tilde{\nabla}\cdot\left[\frac{\tilde{h}^2}{2}\tilde{\nabla}\tilde{\Gamma}_2\right], \tag{4.28}$$

$$\begin{aligned}\partial_{\tilde{t}}\tilde{\Gamma}_1 = {}& \tilde{\nabla}\cdot\left[\frac{\tilde{h}^2\tilde{\Gamma}_1}{2}\tilde{\nabla}\left[W\left(\frac{1}{\tilde{h}^3} - \frac{1}{\tilde{h}^6}\right) - \tilde{\Delta}\tilde{h}\right]\right] + \tilde{\nabla}\cdot\left[\left(\tilde{h}\tilde{\Gamma}_1 + \tilde{D}_1\right)\tilde{\nabla}\tilde{\Gamma}_1\right] + \tilde{\nabla}\cdot\left[\tilde{h}\tilde{\Gamma}_1\tilde{\nabla}\tilde{\Gamma}_2\right] \\ & + \tilde{r}\left[\delta\tilde{\Gamma}_1^2\tilde{\Gamma}_2 - \delta^3\tilde{\Gamma}_1^3\right] - \tilde{\beta}_1\ln(\tilde{\Gamma}_1\delta) - \tilde{\beta\mu},\end{aligned} \tag{4.29}$$

$$\begin{aligned}\partial_{\tilde{t}}\tilde{\Gamma}_2 = {}& \tilde{\nabla}\cdot\left[\frac{\tilde{h}^2\tilde{\Gamma}_2}{2}\tilde{\nabla}\left[W\left(\frac{1}{\tilde{h}^3} - \frac{1}{\tilde{h}^6}\right) - \tilde{\Delta}\tilde{h}\right]\right] + \tilde{\nabla}\cdot\left[\tilde{h}\tilde{\Gamma}_2\tilde{\nabla}\tilde{\Gamma}_1\right] + \tilde{\nabla}\cdot\left[\left(\tilde{h}\tilde{\Gamma}_2 + \tilde{D}_2\right)\tilde{\Gamma}_2\right] \\ & - \tilde{r}\left[\delta\tilde{\Gamma}_1^2\tilde{\Gamma}_2 - \delta^3\tilde{\Gamma}_1^3\right] - \tilde{\beta}_2\ln(\tilde{\Gamma}_2\delta^{-1}) + \tilde{\beta\mu}.\end{aligned} \tag{4.30}$$

The dimensionless wettability parameter

$$W = \frac{Aa_1a_2}{h_a^2k_bT} \tag{4.31}$$

expresses the ratio of wetting energy to surfactant energy. The remaining dimensionless quantities are

$$\delta = \frac{a_1}{a_2}, \tag{4.32}$$

$$\tilde{D}_i = \frac{\eta a_1a_2}{h_a}D_i, \tag{4.33}$$

$$\tilde{r} = \tau a_1a_2 r = \frac{\gamma^0 h_a\eta(a_1a_2)^3}{(k_bT)^2}r, \tag{4.34}$$

$$\tilde{\beta}_i = \tau a_1a_2k_bT\beta_i = \frac{\gamma^0 h_a\eta(a_1a_2)^3}{k_bT}\beta_i, \tag{4.35}$$

$$\tilde{\beta\mu} = \tau a_1a_2\beta\mu = \frac{\gamma^0 h_a\eta(a_1a_2)^3}{(k_bT)^2}\beta\mu. \tag{4.36}$$

In the following, we omit tildes denoting dimensionless quantities.

4.2 Linear Stability Analysis

As a first step to identifying qualitatively different regions in parameter space, we perform a linear stability analysis of the steady states of (4.28)-(4.30) in one spatial dimension. To this

end, a flat film of film height h_0 with the uniform densities $\Gamma_{1,0}$ and $\Gamma_{2,0}$ as solutions to the steady state equations

$$0 = r\left[\delta\Gamma_1^2\Gamma_2 - \delta^3\Gamma_1^3\right] - \beta_1\ln(\Gamma_1\delta) - \beta\mu, \tag{4.37}$$

$$0 = -r\left[\delta\Gamma_1^2\Gamma_2 - \delta^3\Gamma_1^3\right] - \beta_2\ln(\Gamma_2\delta^{-1}) + \beta\mu \tag{4.38}$$

is considered.[3] We also choose the film height of the flat film sufficiently large so that wetting effects are negligible ($h_0 = 20$). The linear behavior of the perturbed state

$$h(x,t) = h_0 + \varepsilon h_1 e^{\lambda t + ikx}, \tag{4.39}$$

$$\Gamma_1(x,t) = \Gamma_{1,0} + \varepsilon\Gamma_{1,1}e^{\lambda t + ikx}, \tag{4.40}$$

$$\Gamma_2(x,t) = \Gamma_{2,0} + \varepsilon\Gamma_{2,1}e^{\lambda t + ikx} \tag{4.41}$$

with $\varepsilon \ll 1$ and $h_1, \Gamma_{1,1}, \Gamma_{2,1} = \mathcal{O}(1)$ is then analyzed by computing the dispersion relation $\lambda(k)$ as eigenvalues of the linearized system. To better understand the transition from the passive system to an active non-equilibrium system with self-organizing properties, the linear behavior of the uniform steady state is analyzed for varying dimensionless reaction rates r and driving forces $\beta\mu$.

Here, we will adopt the following classification of instability types of a uniform steady state (see also Supplementary Material in [FT23] for details). Instabilities are distinguished with respect to three features: large-scale vs. small-scale, stationary vs. oscillatory and conserved vs. non-conserved. An instability is called large-scale (small-scale) if the critical wavenumber k_c is zero (non-zero) at onset. If the frequency of the instability is is zero (non-zero) *near* onset, the instability is called stationary (oscillatory). Finally, if the dominant mode corresponds to a conservation law there must exist at least one neutral mode with $\lambda = 0$ at $k = 0$ for all parameter values. Then the instability mode is called conserved, otherwise it is called non-conserved. This convention is summarized in Tab. 4.1 where each instability feature is assigned a symbol. In total, eight different types of instabilities are differentiated. Before proceeding, we will give some examples of well-known (and not so well-known) instability types and discuss how they are classified in the present scheme. For instance, a standard Turing instability is a non-conserved stationary small-scale instability (symbol: S_n^s). A Hopf instability corresponds to a non-conserved oscillatory large-scale instability (symbol: L_n^o). There also exist conserved counterparts. A "conserved Turing instability" is classified as a conserved stationary small-scale instability (symbol: S_c^s) and may e.g. occur in three-field reaction-diffusion systems with a conservation law. Additionally, there exists a "conserved Hopf instability" which corresponds to a conserved oscillatory large-scale instability (symbol: L_c^o). An instability of this type may be found in systems with two or more conservation laws. Since Eqs. (4.28)-(4.30) only conserve one quantity, the liquid volume, such an instability is excluded in the present system.

[3] In the following analysis, $\delta = 1$ is used. Eqs. (4.37) and (4.38) then have the trivial solution $\Gamma_1 = \Gamma_2 = 1$ for $\beta\mu = 0$. In Fig. 4.2, this solution is then "continued" for greater values of $\beta\mu$ by using the solution at a previous value as an initial guess.

Table 4.1: Classification of instability types with respect to three features of the instability: spatial modulation, temporal modulation and whether the instability corresponds to a conservation law in the system. For an extensive discussion, see [FT23].

Category	Type	Symbol
spatial modulation	large-scale	L
	small-scale	S
temporal modulation	stationary	s
	oscillatory	o
conservation properties	conserved	c
	non-conserved	n

In the plane spanned by the reaction rate r and the driving force $\beta\mu$, different instability regimes may be identified by their *dominant* instability mode, determined by the maximum real part of the dispersion relation. The dominant modes are classified accordingly to the described scheme. Note that since the linear behavior is considered here in a parameter *plane* the notion of onset is somewhat ambiguous, however, we find that the dispersion relations are usually a superposition of clearly distinct instabilities which can identified with any of the eight considered types. We also remark that the distinction between S_c^s- and S_n^s-type instabilities is carried out by manual inspection of the dispersion relations. Corresponding points are marked by black crosses in the r-$\beta\mu$-plane.

The different stability regimes are shown in Fig. 4.2a. The flat film shows a L_c^s instability for small driving forces and fast reactions (large r). This instability is associated with the coarsening of the uniform state into a single drop or bubble in passive systems like the simple thin-film equation or the Cahn-Hilliard model [Gla+09; Arg+05]. In active systems (here $\beta\mu \neq 0$) coarsening may be suppressed, even if the dispersion relation indicates a L_c^s instability [FWT21]. If the driving force $\beta\mu$ is further increased, a Hopf instability can be observed (L_n^o). For even greater values of $\beta\mu$, the dominant instability mode is Turing-like (S_n^s). For smaller reaction rates and large driving forces, the dominant instability corresponds to a non-conserved stationary large-scale instability (L_n^s). The stability diagram changes if the diffusion coefficients $D_{1,2}$ are varied. If Γ_2 diffuses fast, except for the L_c^s-region all dominant modes are stationary small-scale instabilities (Fig. 4.2b). In addition to the previously observed non-conserved Turing-region (S_n^s), a conserved Turing-region (S_c^s) now separates the S_n^s-region from the L_c^s-region. Conversely, for a fast diffusing Γ_1 we only find large-scale instabilities (Fig. 4.2c). The circumstance that diffusion may drastically influence the stability of spatially extended systems has already been known since Turing's seminal article [Tur52]. In this particular case, it can be explained by understanding the autocatalytic reaction

$$2\Gamma_1 + \Gamma_2 \rightleftharpoons 3\Gamma_1 \tag{4.42}$$

as a conversion reaction with a reaction rate that is modulated by Γ_1^2. Therefore, spatial compartments with different values of Γ_1 differ greatly in conversion speeds so that spatial pattern formation is facilitated. However, if Γ_1 diffuses fast it will be distributed approximately homogeneously in space so that no small-scale instability occurs.

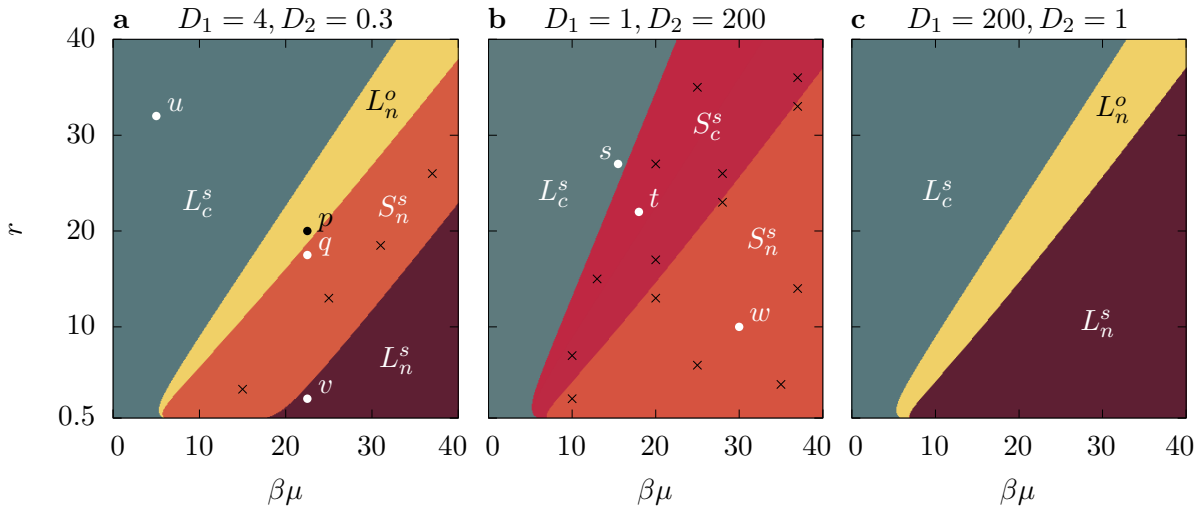

Figure 4.2: Instability regimes of a flat film in the r-$\beta\mu$-plane for different diffusion coefficients: **a** $D_1 = 4, D_2 = 0.3$, **b** $D_1 = 1, D_2 = 200$ and **c** $D_1 = 200, D_2 = 1$. The remaining parameters are $W = 1$, $\delta = 1$, $\beta_1 = 6$ and $\beta_2 = 1$. Note that S_c^s- and S_n^s-type instabilities are distinguished manually by inspecting the dispersion relations at the points marked with black crosses. Labeled points denote parameter combinations for which the dispersion relations are shown in Figs. 4.3-4.5.

To illustrate the results in Fig. 4.2, we also show the dispersion relations at selected points in the r-$\beta\mu$-plane (Figs. 4.3-4.5). Figs. 4.3a, b correspond to u in Fig. 4.2a, where the weak L_c^s instability can be seen for small wavenumbers (inset in Fig. 4.3a). At v, the dominant instability mode is of type L_n^s and the dispersion relation is real for all shown k (Figs. 4.3c, d). The transition from the L_n^o-region to S_n^s-region can be seen in the changes in dispersion relations from p to q. At both points, the dominant mode is a superposition of a standard Hopf and a standard Turing instability (L_n^o and S_n^s). At p, the Hopf mode is dominant (Figs. 4.4a, b) while at q the Turing mode is dominant (Figs. 4.4c, d). The dispersion relations at the points in Fig. 4.2b are presentend in Fig. 4.5. At s, the flat film is again weakly L_c^s-unstable. At t the dominant mode is then a conserved Turing instability (S_c^s) (Figs. 4.5c, d) which corresponds to the same eigenvalue as the L_c^s instability (see also insets in Figs. 4.5a, c). At w, the dominant mode is of S_n^s-type (non-conserved Turing, Figs. 4.5e, f). Note that in all shown dispersion relations, there always exists the underlying weak L_c^s instability, even when the dominant instability is of a different type.

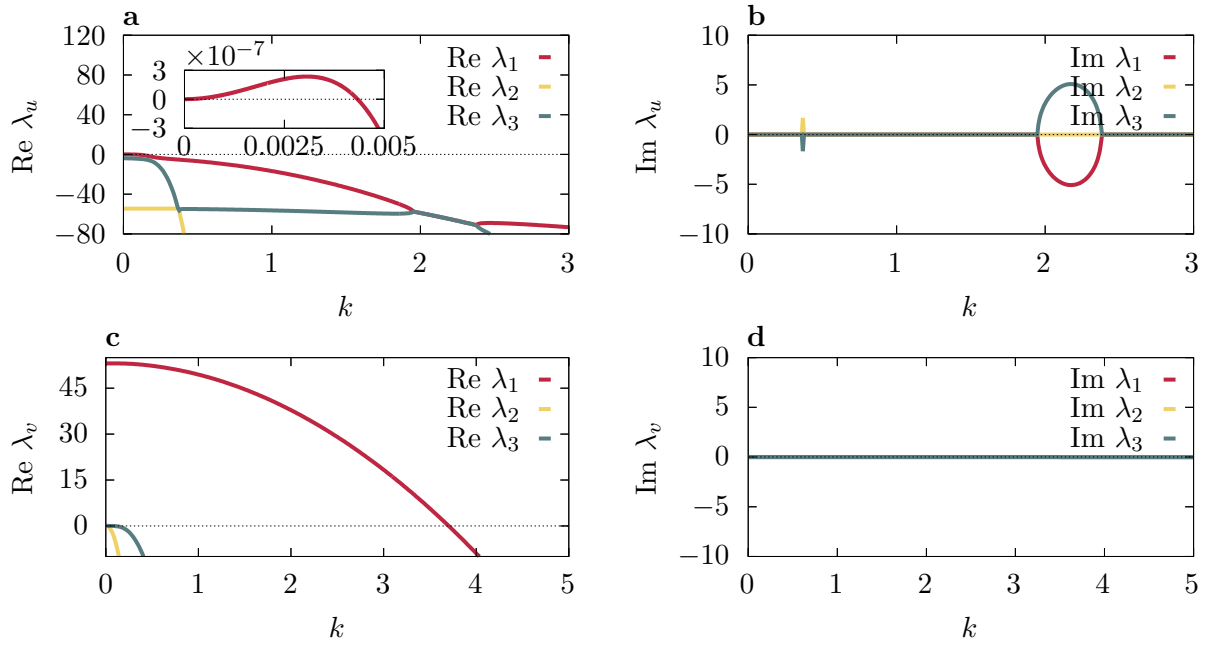

Figure 4.3: Real and imaginary parts of the dispersion relations at the points u (**a**, **b**) and v (**c**, **d**) in Fig. 4.2a. The inset in **a** shows the weak L_c^s instability. As a visual cue, a dashed base line is drawn.

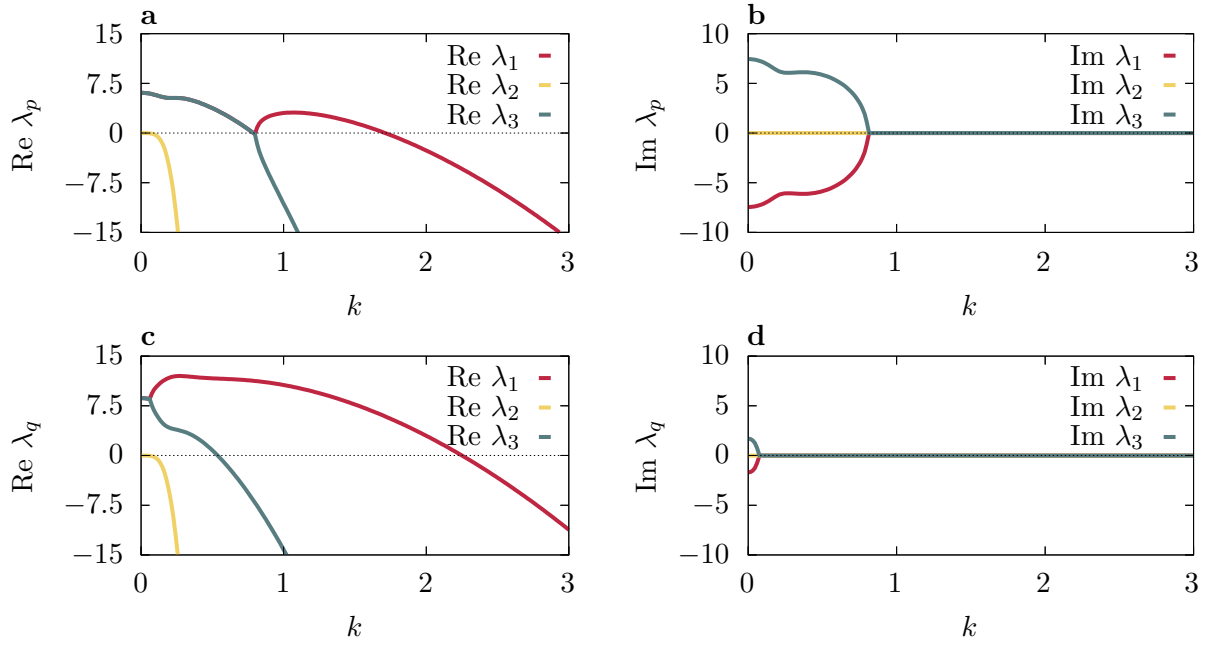

Figure 4.4: Real and imaginary parts of the dispersion relations at the points p (**a**, **b**) and q (**c**, **d**) in Fig. 4.2a. As a visual cue, a dashed base line is drawn.

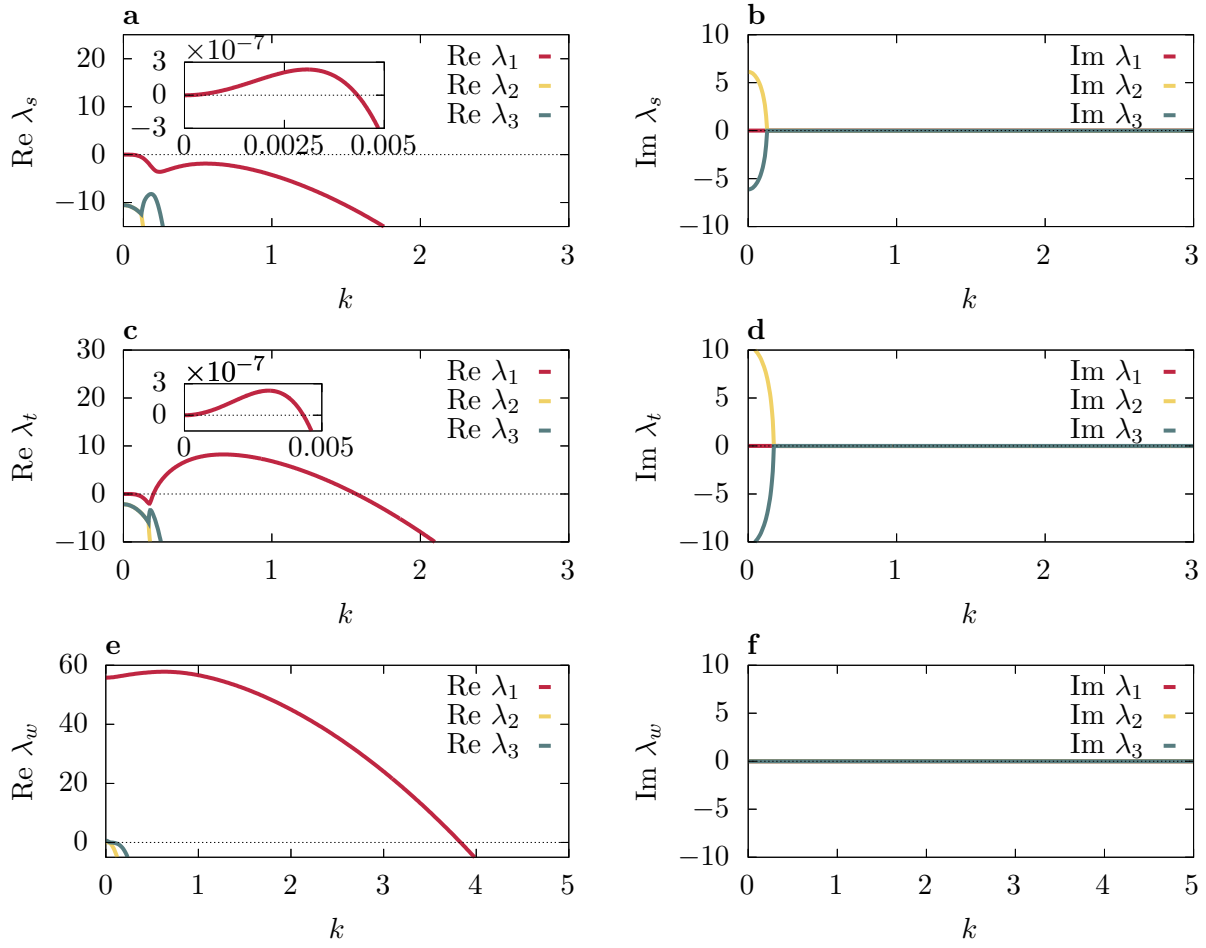

Figure 4.5: Real and imaginary parts of the dispersion relations at the points s (**a**, **b**) and t (**c**, **d**) and w (**e**, **f**) in Fig. 4.2b. The insets in **a** and **c** show the weak L_c^s instabilities. As a visual cue, a dashed base line is drawn.

4.3 Numerical Continuation and Time Simulations

While the foregoing linear stability analysis has shown that Eqs. (4.28)-(4.30) allow for the formation of spatial and temporal patterns, particularly for large driving forces, it is insufficient for understanding the full non-linear behavior of the model. To this end, we analyze the model using numerical continuation in PDE2PATH [Uec21] as well as finite-element time simulations in OOMPH-LIB [HH06], when suitable. In particular, some standing waves found in time simulations are further analyzed with numerical continuation to produce bifurcation diagrams that can be directly linked to the observed solutions in time simulations.

In the bifurcation diagrams, the following conventions are adopted. As a solution measure, we use the L_2-norm of the film height

$$||h||_2 = \sqrt{\frac{1}{L}\int_{-L/2}^{L/2} h^2 \,\mathrm{d}x} \tag{4.43}$$

with the domain size L. For time-periodic states with period T, the time-averaged norm $1/T \int_0^T ||h||_2 \,\mathrm{d}t$ is used, instead. Unless stated otherwise, the shown results are obtained for a one-dimensional periodic domain of size $L = 100$ and with a drop volume of

$$V = \int_{-L/2}^{L/2} h \,\mathrm{d}x \approx 816.1. \tag{4.44}$$

The driving force $\beta\mu$ which was introduced in Eq. (4.21) is used as the primary continuation parameter as it directly measures how strongly the system is driven away from equilibrium. As a base branch, a stationary single drop with uniform surfactant densities, determined by Eqs. (4.37) and (4.38), is a natural choice. We differentiate bifurcation classes using symbols. Solution branches of different types are distinguished by colors, while stability properties are encoded as line types. Linearly stable branches are drawn as solid lines, while unstable branches are represented by dashed lines. The base branch is drawn in black. A partial summary of the symbol and color scheme is given in Tab. 4.2.

Table 4.2: Summary of symbol and color conventions used in bifurcation diagrams to differentiate bifurcation and solution types.

Symbol	Current Branch	Bifurcation Type	Emerging Branch (Branch Color)
○	steady state	unspecified (see Sec. 4.3.1)	steady state (■)
	standing wave	pitchfork/transcritical bif. of standing waves	standing wave (■)
◊	steady state	Hopf	standing wave[4] (■)
	standing wave	torus	quasi-per. standing waves (none)
▲	steady state	drift-pitchfork	traveling drop (■)
	standing wave	drift-pitchfork of standing waves	modulated traveling drop (■)

When discussing results of the time simulations, we also use the full L_2-norm

$$||\psi||_2 = \sqrt{\frac{1}{L}\int_{-L/2}^{L/2} \left[h^2 + p^2 + \Gamma_1^2 + \Gamma_2^2\right] \, \mathrm{d}x}, \tag{4.45}$$

where the pressure p is given by Eq. (4.20). Additionally, to study the differences between distinct modes of drop oscillation, we introduce the center of mass $\langle x \rangle$ and its period-average x_0, where[5]

$$\langle x \rangle = \frac{1}{V}\int_{-L/2}^{L/2} xh \, \mathrm{d}x, \tag{4.46}$$

$$x_0 = \frac{1}{T}\int_0^T \langle x \rangle \, \mathrm{d}t. \tag{4.47}$$

The corresponding displacement Δx is then defined as

$$\Delta x = \langle x \rangle - x_0. \tag{4.48}$$

It is used as a central measure for the distinction of different types of oscillatory modes.

Generally, Eqs. (4.28)-(4.30) turn out to possess quite rich behavior including oscillating, traveling and modulated traveling drops. The detailed results of combined numerical continuation and time simulations are presented in the following. First, the discussion focuses on steady states as well as on oscillating and traveling drops. Additionally, first results regarding modulated traveling drops are given in Sec. 4.3.2. Finally, we classify different modes of drop oscillation in Sec. 4.3.3.

[4] If the base branch is uniform and the system has translational symmetry, standing waves may emerge together with traveling waves. Here, we always consider drop solutions so that no traveling waves may emerge from a Hopf bifurcation.

[5] Note that Eq. (4.46) formally defines the geometric center of the drop (or rather, its x-coordinate). However, in the thin-film approximation a homogeneous, incompressible fluid is treated and the two quantities coincide.

4.3.1 Steady, Oscillating and Traveling Drops

To reveal parts of the typical branching structure of a simple drop, we first consider a combination of parameters that is "not too complicated". The corresponding bifurcation diagram is shown in Fig. 4.6a and solutions at selected points are presented in Fig. 4.7. As the driving force $\beta\mu$ is increased, the simple drop solution (black) becomes unstable and two branches of unstable drop states with patterned surfactants (blue) emerge subcritically, i.e., in the direction of the linearly stable branch. Here, two real eigenvalues cross the imaginary axis (cf. stability information in Fig. 4.6a) and the emerging one- and two-peak branches posses one and two unstable eigenvalues, respectively. This type of instability seems closely related to the emergence of localized states in homoclinic snaking on periodic domains, where two branches of localized symmetric states with distinct phase emerge from a periodic state [BK07; Ber+08; HK09].[6] However, while the surfactant profiles of the emerging branches are similar to the localized states in homoclinic snaking (cf. Fig. 4.7a), the present instability seems distinct since the branches bifurcate from an *aperiodic* base state. Therefore, while expecting two subcritical pitchfork branches similarly to homoclinic snaking, we here leave the bifurcation class unspecified. Nevertheless, we will refer to states that emerge from such a bifurcation as "fully localized", in analogy to the localized states found in homoclinic snaking. In the present case, both branches of fully localized states become stable in saddle-node bifurcations and are interconnected by two branches of asymmetric traveling drops (orange), which are related by reflection symmetry. They connect to the two steady branches in supercritical drift-pitchforks (filled triangles, see also Fig. 4.6b) [Gol+91; FDT91], where the traveling drops connect to the two-peak branch after a fold (Fig. 4.6i). Note that there exists a small parameter region where the simple drop, the two-peak branch and the traveling drop branches are simultaneously stable. With increasing $\beta\mu$ the two-peak branch folds into a three-peak branch in a saddle-node bifurcation and then connects to the base branch subcritically. Here, a four-peak branch emerges supercritically.[7] Also, from the three-peak branch, traveling drops emerge in a supercritical drift-pitchfork. Note that this bifurcation is located just after a fold (see stability information in Fig. 4.6a).

[6] This is for the case of models with the reflection symmetry $\mathcal{R} : (-x, \phi) \mapsto (x, \phi)$ but *without* the inversion symmetry $\mathcal{I} : (-\phi) \mapsto (\phi)$. Therefore, the two emerging branches are not related by symmetry. Note that Eqs. (4.28)-(4.30) are also not left invariant under the inversion of any of the fields, or any combinations thereof, but are invariant under reflection.

[7] Note that since two real eigenvalues of the base branch cross the imaginary axis in this bifurcation and because the sub- and the supercritical branch possess the same number of unstable eigenvalues (see stability information in Fig. 4.6a), a transcritical bifurcation can be ruled out. We expect this bifurcation to be of the same class as the bifurcation of the first two steady branches.

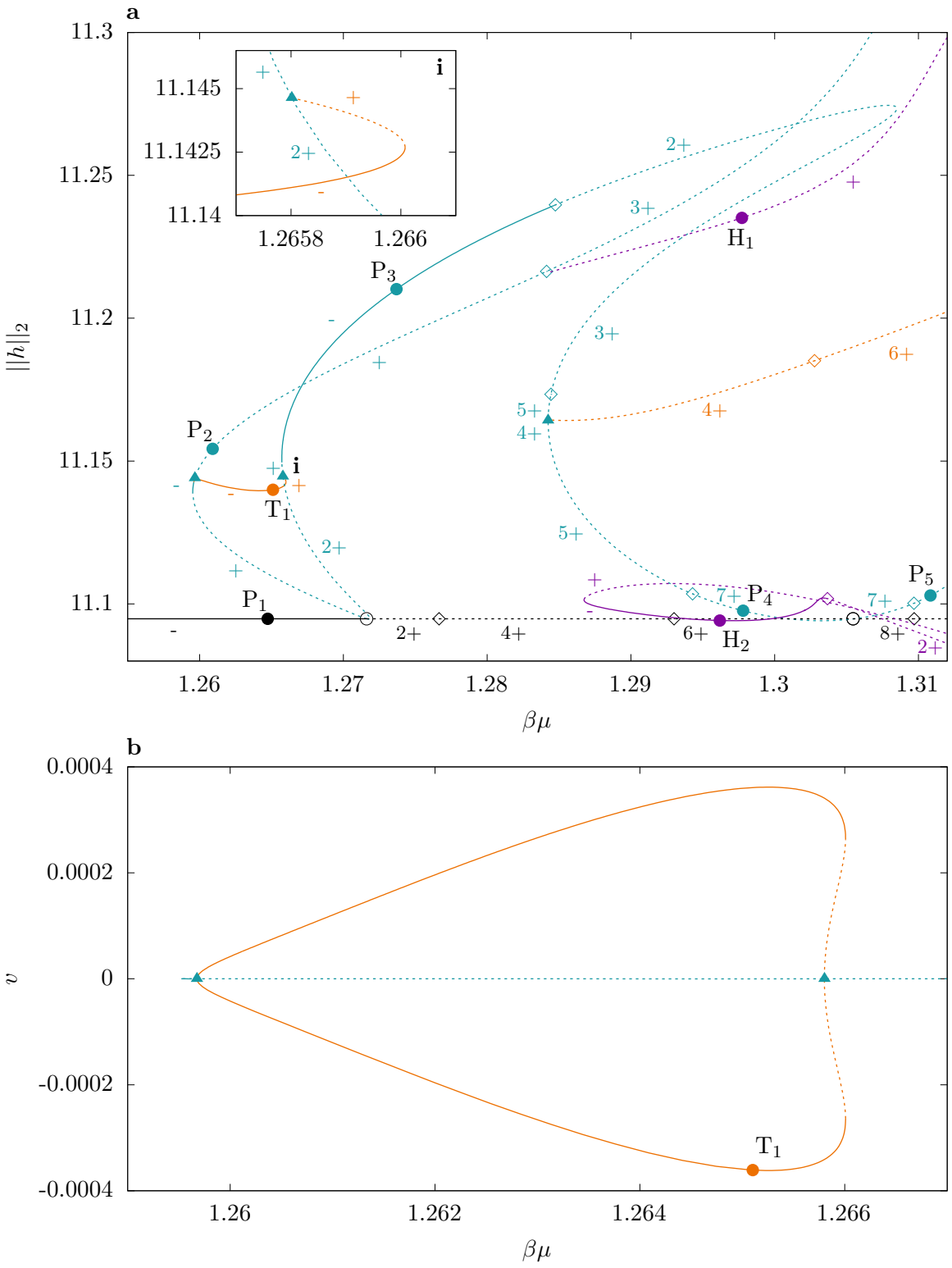

Figure 4.6: **a** Partial bifurcation diagram of the simple drop solution (black) in the driving force $\beta\mu$. The remaining parameters are $W = 3, \delta = 1, D_1 = 1.4, D_2 = 0.1, r = 0.8, \beta_1 = 1$ and $\beta_2 = 0.5$. Blue branches correspond to fully localized steady states, orange branches to traveling drops and purple branches to standing waves of drops. Filled circles denote selected points at which solutions are plotted in Fig. 4.7. Linearly stable branches are marked with "-", for unstable branches the number n of unstable eigenvalues/Floquet multipliers is given by "n+". The inset **i** shows the saddle-node bifurcations of the first traveling drop branches (left- and right traveling, same norm here). **b** Supercritical drift-pitchfork bifurcations of the first two traveling drop branches from the steady state branches. Shown is the speed v of the comoving frame in which the solutions are stationary, versus the driving force $\beta\mu$.

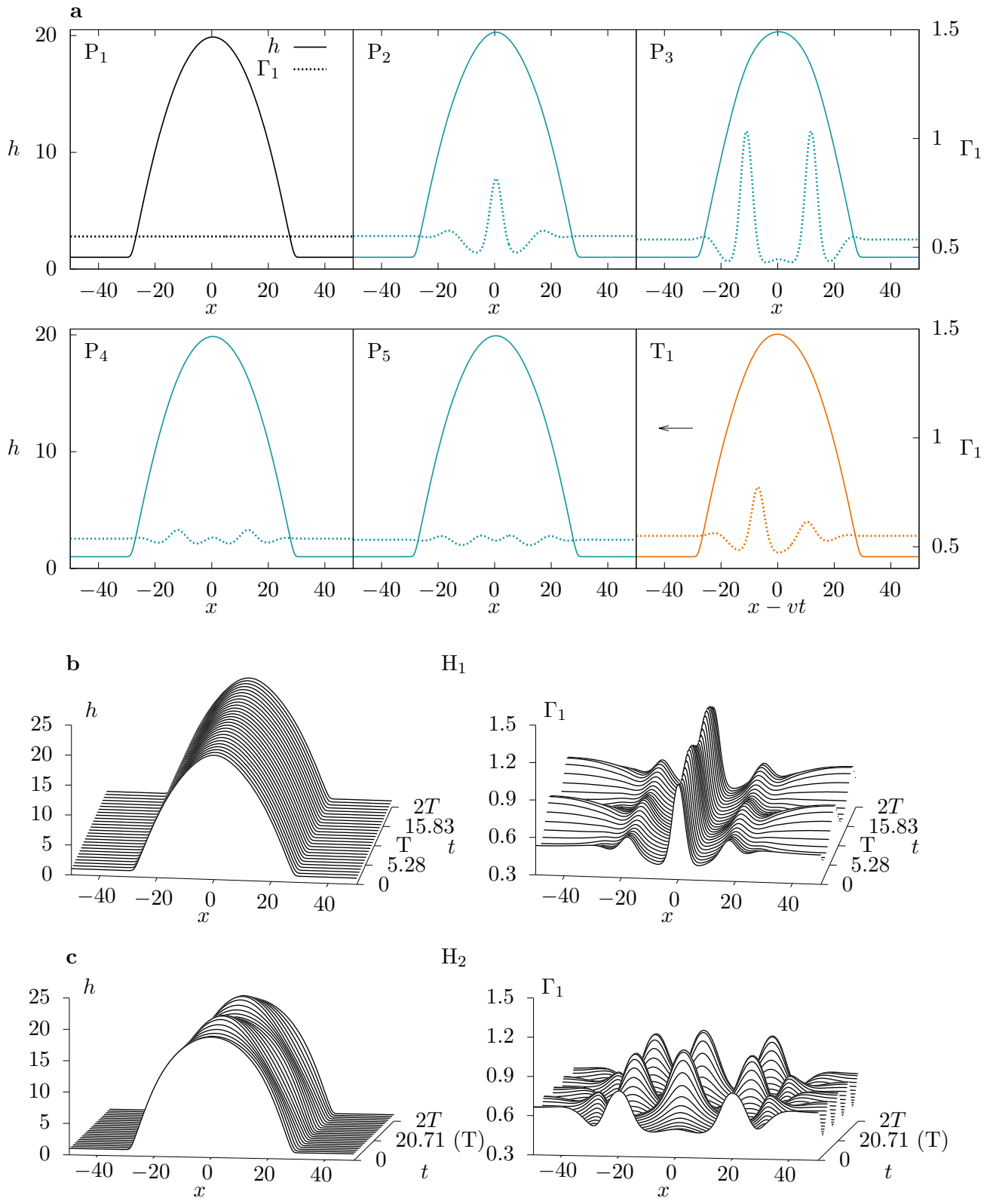

Figure 4.7: **a** Solution profiles of the film height h and the surfactant Γ_1 at the points marked in Fig. 4.6. The traveling drop is shown in the comoving frame with speed v, the arrow indicates direction of travel. **b**, **c** Oscillating drops at the points H_1 and H_2 in Fig. 4.6**a**. Shown are the film height h and the surfactant Γ_1 over a span of two periods. On the t axis, tick marks indicate $T/2, T, 3/2T$ and $2T$. The respective values are rounded to two decimal places.

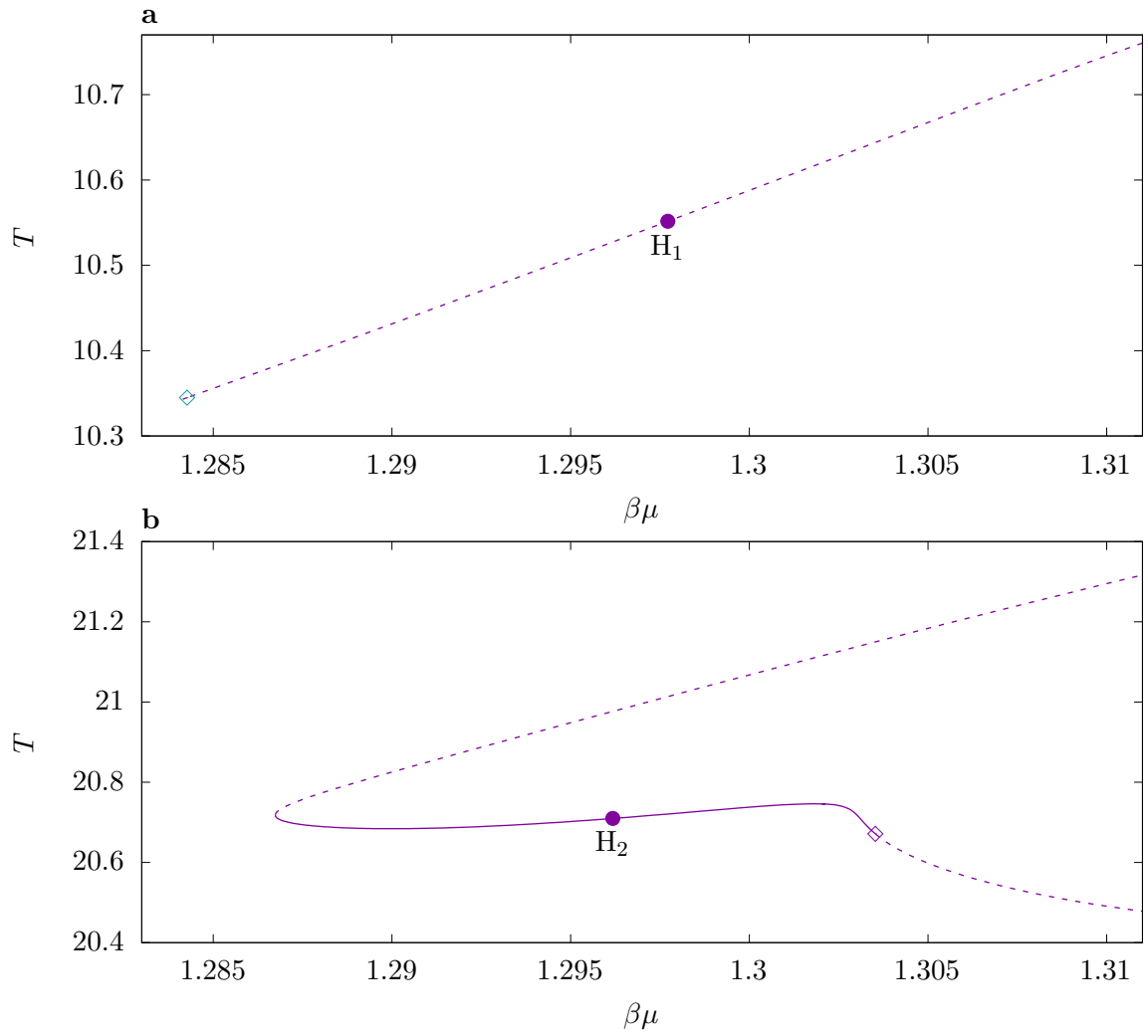

Figure 4.8: Periods T of the oscillating drops shown in Fig. 4.6. **a** corresponds to the unstable branch that connects to the one-peak branch in a Hopf bifurcation. **b** is associated with the partially linearly stable standing wave branch.

In addition to the previously described steady and traveling states, there also exist a number of Hopf bifurcations on all branches in which oscillating drops or, from the traveling drops, modulated traveling drops may appear. The purple branches shown in Fig. 4.6a correspond to standing waves of drops that were continued from time simulation data. The solutions at $H_{1,2}$ are visualized in Figs. 4.7b, c. The first (Hopf) branch is traced back to a Hopf bifurcation from the one-peak branch and corresponds to axisymmetric surfactant oscillations (with respect to parity) which barely couple to the drop (Fig. 4.7b). Its period increases linearly with the driving force (Fig. 4.8a). The Hopf branch remains unstable, however, the deviation of the associated Floquet multiplier from the unit circle is of the order 10^{-2} so that the solutions can be found as transients in time simulations. Here, a further numerical study is needed to determine the states that are ultimately approached for large t. The second branch of oscillating drops comprises noticeable axisymmetric oscillations in all three fields (Fig. 4.7c). The branch is linearly stable in a limited parameter range and is rendered unstable in a fold of standing waves and in a torus bifurcation, respectively. In the stable range, the corresponding period barely changes. However, as $\beta\mu$ is increased the period increases approximately linearly after the fold and also decreases significantly after the torus bifurcation. Also note that this branch is not traced back to any of the shown Hopf bifurcations but continues toward large $\beta\mu$.

While the bifurcation structure of the simple drop shown in Fig. 4.6a is comparatively simple,

many of its features seem to be of general nature and can also be found for more "complicated" choices of parameters. An example is shown in Fig. 4.9, where solutions at selected points are again displayed in Fig. 4.10. Here, the simple drop first becomes unstable in a Hopf bifurcation. Fully localized states then emerge subcritically from the base branch in the same bifurcation class as in the previous case and they are again connected by traveling drop branches that appear in drift-pitchforks. The respective speeds of some of the branches are displayed in Figs. 4.11a, b. In both cases, the generic drift-pitchfork structure can be observed close to the respective bifurcation. Here, the traveling drops connecting the one- and two-peak branches show a more complex branching structure due to saddle-node bifurcations further away from the bifurcations (Fig. 4.11a). Also, for the branches of fully localized steady states we see that starting from the two-peak branch, branches with even peak numbers and branches with odd peak numbers are connected by the branching structure. All fully localized states and all traveling drop states are unstable.

Besides the steady and traveling drops, we continue an oscillating drop state from time simulations, showing pronounced axisymmetric drop oscillations (purple branch, see also Fig. 4.10b). The branch is linearly stable in a limited parameter region and turns unstable in either a pitchfork or a transcritical bifurcation of standing waves for decreasing $\beta\mu$. As $\beta\mu$ is increased, the branch is rendered unstable in a torus bifurcation. Time simulations just beyond this bifurcation also show (quasi-)periodic solutions that can be identified by beats in the full L_2-norm $||\psi||_2$ (Fig. 4.12). In fact, for even higher values of $\beta\mu$, only solutions of this kind were found in time simulations. The period T of the branch is shown in Fig. 4.11c. It increases after the pitchfork/transcritical bifurcation of standing waves and decreases after the torus bifurcation that renders the branch unstable. Also note that the purple branch is bordered by two drift-pitchforks of standing waves (purple triangles). They do not mark the ends of the branch, but continuation was stopped at both bifurcation points. We give some results regarding the emerging branches of modulated traveling drops in Sec. 4.3.2.

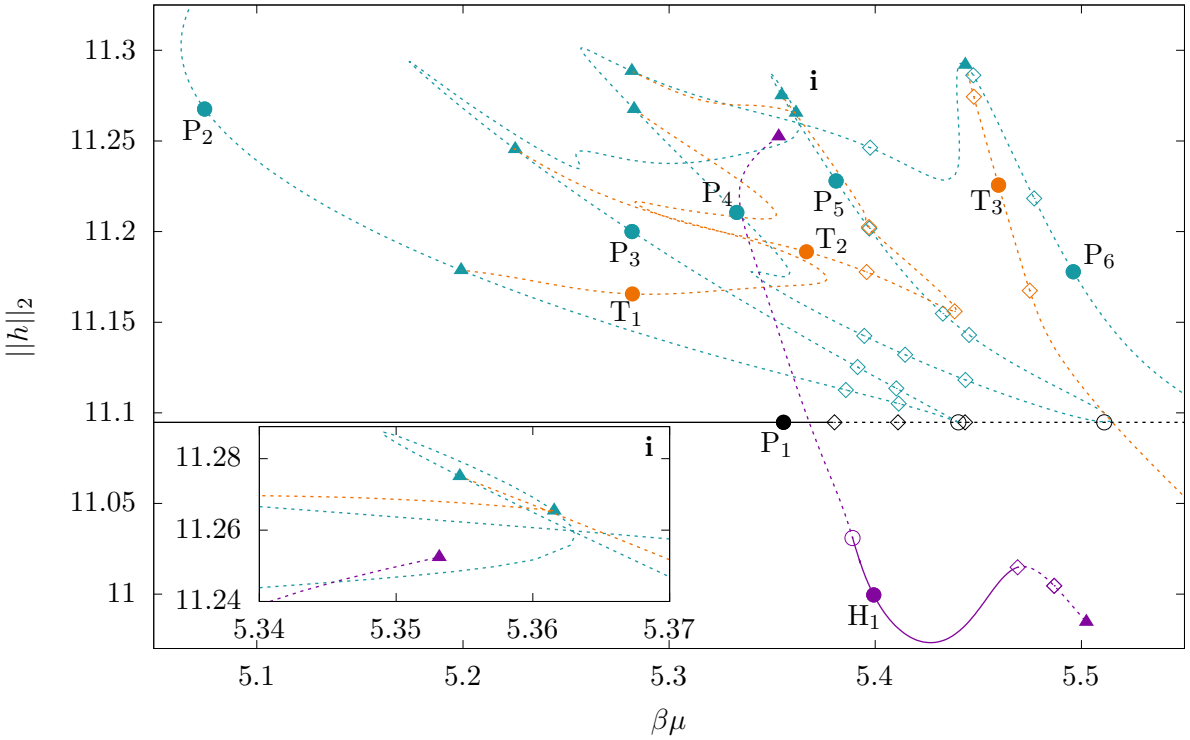

Figure 4.9: Partial bifurcation diagram of the simple drop solution (black) in the driving force $\beta\mu$. The remaining parameters are $W = 3, \delta = 1, D_1 = 2, D_2 = 0.15, r = 1.1, \beta_1 = 6$ and $\beta_2 = 1$. Blue branches correspond to fully localized steady states, orange branches to traveling drops and purple branches to oscillating drops (standing waves). Filled circles denote selected points at which solutions are plotted in Fig. 4.10. The inset **i** shows a zoom of the marked region.

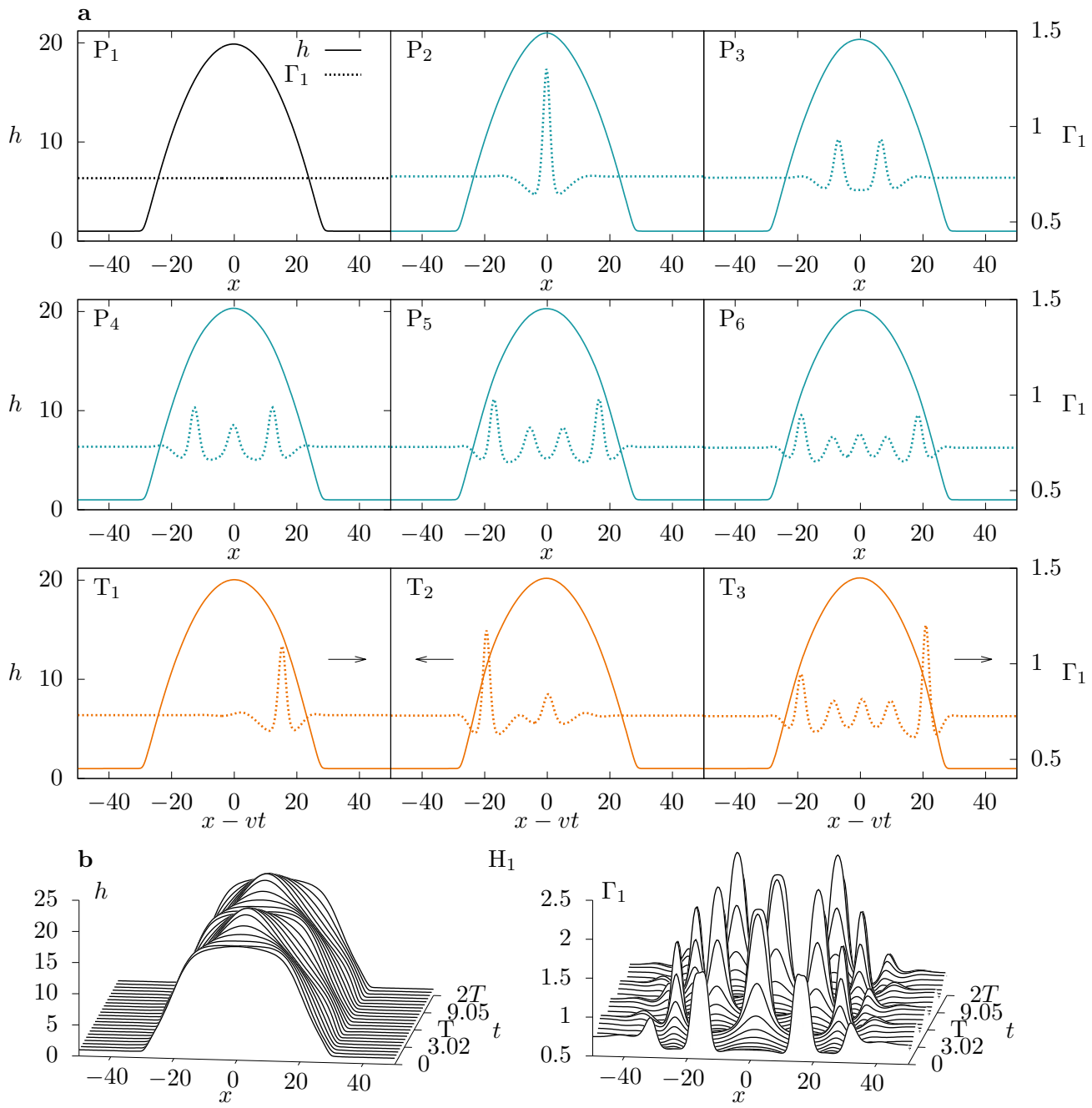

Figure 4.10: **a** Solution profiles of the film height h and the surfactant Γ_1 at the points marked in Fig. 4.9. Traveling drops are shown in the comoving frame with speed v, arrows indicate directions of travel. **b** Oscillating drop at the point H_1 in Fig. 4.9. Shown are the film height h and the surfactant Γ_1 over a span of two periods. On the t axis, tick marks indicate $T/2, T, 3/2T$ and $2T$. The respective values are rounded to two decimal places.

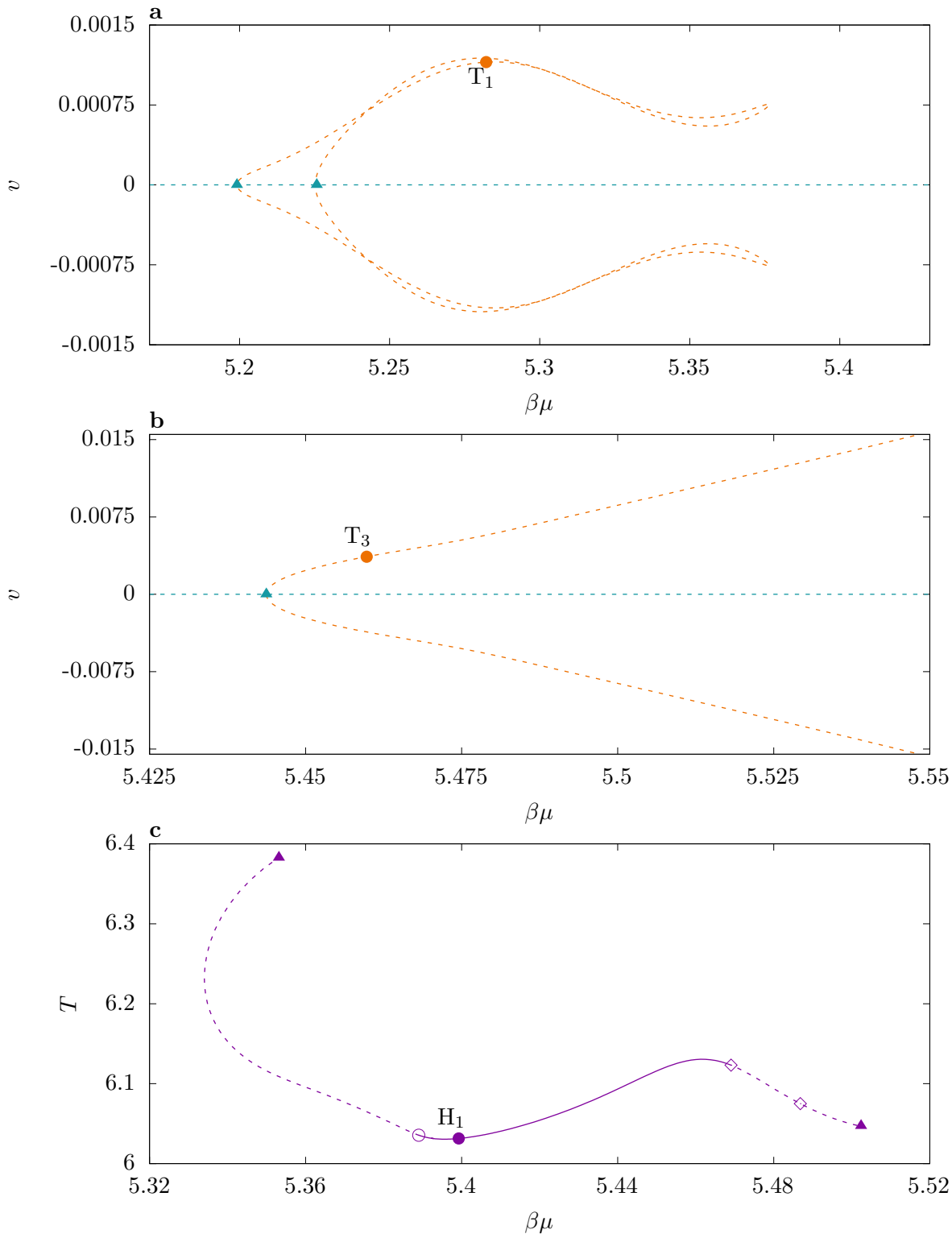

Figure 4.11: **a, b** Speeds v of some of the traveling drop branches in Fig. 4.9. **a** shows the branches connecting the fully localized one- and two-peak states. **b** shows the branches emerging from the fully localized five-peak branch. In **a** and **b**, no bifurcation points except the respective drift-pitchforks are shown. **c** Period T of the oscillating drop in Fig. 4.9.

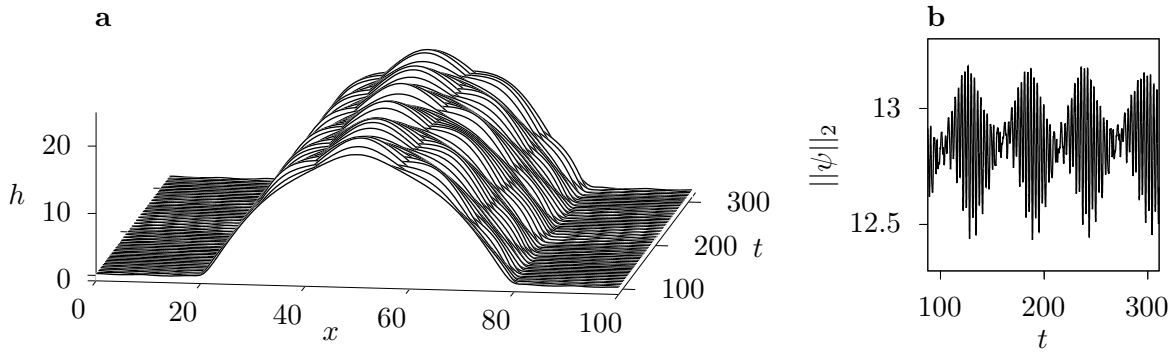

Figure 4.12: **a** (Quasi-)periodic time evolution of a drop, obtained from time simulations at $W = 3$, $D_1 = 2, D_2 = 0.15, r = 1.1, \beta_1 = 6, \beta_2 = 1$ and $\beta\mu = 5.48$. **b** The time evolution of the full L_2-norm shows a beat, indicating that the solution is located on a torus orbit.

Finally, it is pointed out that besides the shown axisymmetric modes of drop oscillations, there also exist anti-axisymmetric modes (with respect to parity). As an example, an unstable mode obtained from a different continuation run is given in Fig. 4.13. Here, the drop oscillates from left to right and back, over the course of one period. We give a quantitative classification of oscillatory modes in Sec. 4.3.3.

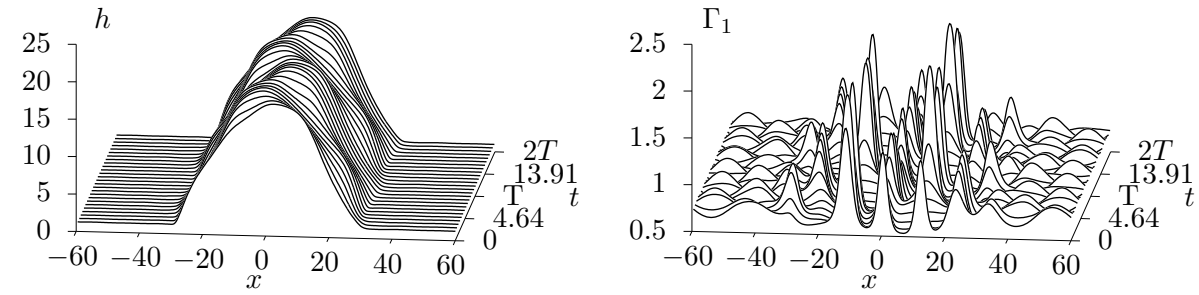

Figure 4.13: Unstable anti-axisymmetric drop oscillation obtained from continuation on a periodic domain with $L = 120$ and $V = 720$. The remaining parameters are $W = 1.504, \delta = 1, D_1 = 4$, $D_2 = 0.3, r = 1.2, \beta_1 = 6, \beta_2 = 1$ and $\beta\mu = 5.7868$. Shown are the time evolution of the film height h and the surfactant Γ_1 over a span of two periods. On the t axis, tick marks indicate $T/2, T, 3/2T$ and $2T$. The respective values are rounded to two decimal places.

4.3.2 Modulated Traveling Drops

As previously described, Eqs. (4.28)-(4.30) allow for modulated traveling drops. For instance, corresponding unstable branches appear from the drift-pitchforks of standing waves that were mentioned in Sec. 4.3.1. The standing wave branch (purple), together with the emerging branches of modulated traveling drops (red), is again shown in Fig. 4.14a. The right-traveling state at mT_1 is displayed in the comoving frame in Fig. 4.14b. Note that similarly to the simple traveling drops, the reflection symmetry of the solution is broken and the droplet oscillates asymmetrically. The periods and speeds of the emerging modulated traveling drop branches are shown in Fig. 4.15. For the second drift-pitchfork (located at $\beta\mu \approx 5.5$), we see that the speeds approach zero for increasing values of $\beta\mu$. Therfore, we expect either another drift-pitchfork bifurcation or a change of sign in the speed, corresponding to an exceptional point at which possibly resting, asymmetrically oscillating drops may be found. This merits further investigation of the emerging traveling branches. We also note that stable modulated traveling drops are found in time simulations (Fig. 4.16). Therefore, Eqs. (4.28)-(4.30) possess *(linearly) stable*

solutions in the form of traveling and modulated traveling drops that correspond to *directional transport of bulk liquid as a result of spontaneous symmetry breaking.*

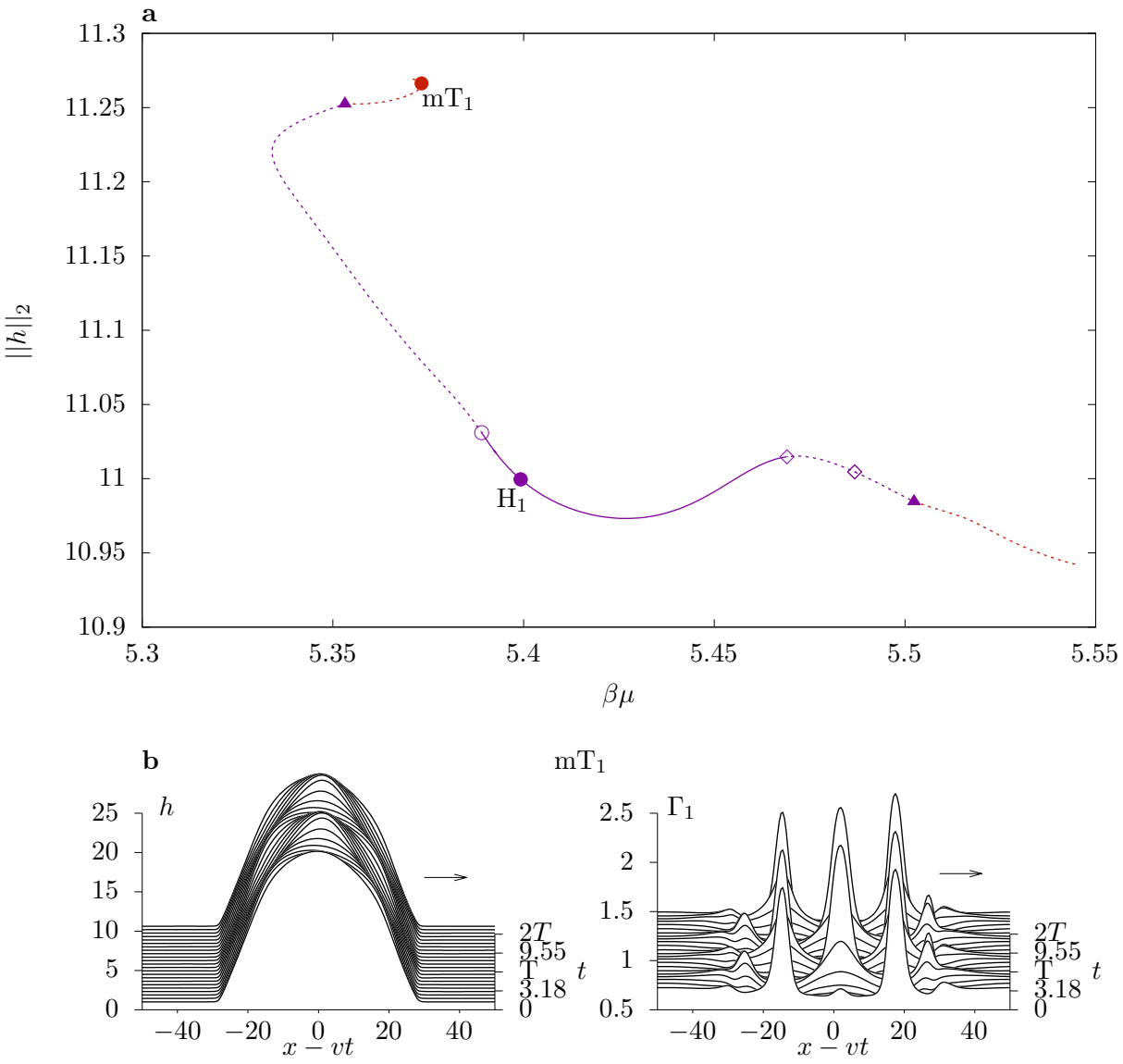

Figure 4.14: **a** Branch of standing waves (purple) from Fig. 4.9 with branches of modulated traveling drops (red) emerging from drift-pitchfork bifurcations of standing waves (purple triangles). Note that the standing wave branch was only continued up to the drift-pitchforks. **b** The time evolution of the right-traveling state at mT$_1$ is shown in the comoving frame with speed v. Here, the film height h and the surfactant Γ_1 are displayed over the course of two periods. On the t axis, tick marks indicate $T/2, T, 3/2T$ and $2T$. The respective values are rounded to two decimal places.

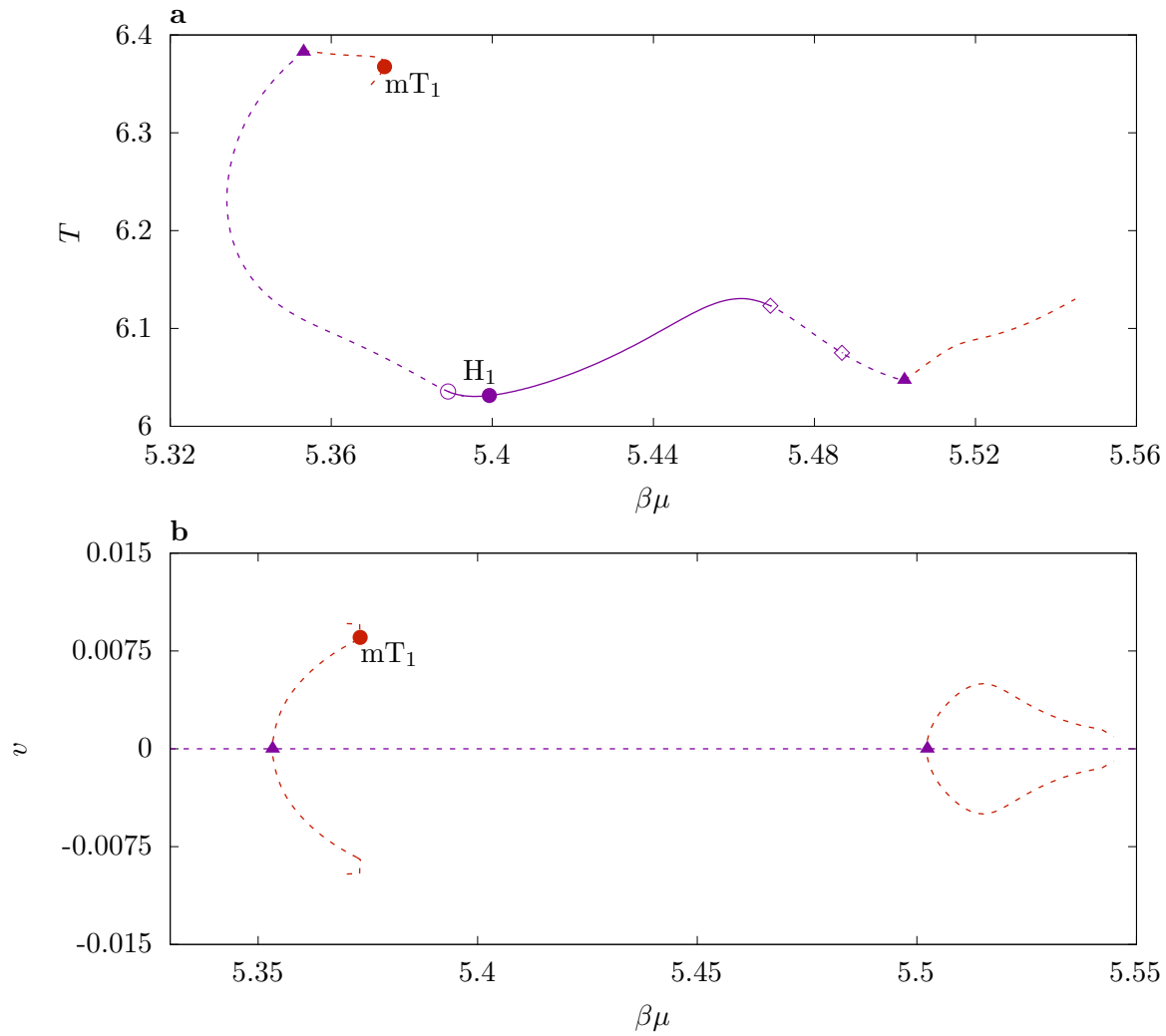

Figure 4.15: **a** Period T of the oscillating drop branch (purple) and the modulated traveling drop branches (red, in the comoving frame) from Fig. 4.14. **b** The modulated traveling drops (red) emerge from drift-pitchfork bifurcations of standing waves (purple triangles) in Fig. 4.9. Shown is the speed v of the comoving frame. Besides the drift-pitchforks of standing waves, no bifurcations are shown explicitly in **b**.

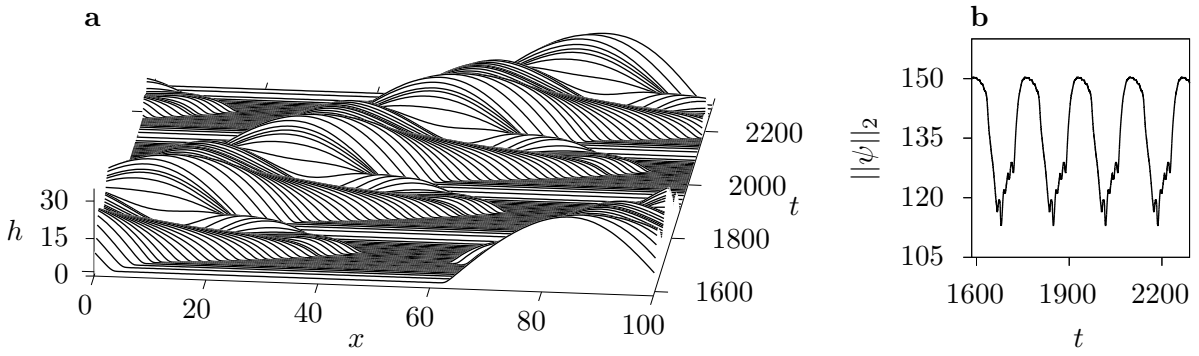

Figure 4.16: **a** Film height evolution of a modulated traveling drop found in time simulations (laboratory frame) at $W = 7, D_1 = 1.3, D_2 = 0.1, r = 0.8, \beta_1 = 1.4, \beta_2 = 0.7$ and $\beta\mu = 2.2$. **b** Corresponding time evolution of the full L_2-norm. Since the L_2-norm is invariant under spatial translation, it oscillates with the frequency of the solution in the comoving frame.

4.3.3 Classification of Oscillatory Modes

Finally, we classify the previously described forms of drop oscillation by the respective displacement Δx of the drop center of mass, defined in Eq. (4.48). To this end, three mode types are distinguished with respect to parity: axisymmetric, anti-axisymmetric and asymmetric modes. The characteristic space-time plots of each mode type are shown in Fig. 4.17, where some of the previously shown solutions are used as examples. For axisymmetric modes (Fig. 4.17a-c), the displacement remains zero, $\Delta x(t) = 0$, as time progresses, i.e., the drop center of mass always coincides with its period-averaged value. For anti-axisymmetric modes (Fig. 4.17d), the displacement symmetrically oscillates about zero, without any preference in spatial direction. In particular, the symmetry

$$\Delta x(t + T/2) = -\Delta x(t) \tag{4.49}$$

holds. In fact, it can be observed that after half a period, the drop profile is the reflection of its previous counterpart. The corresponding line of reflection perpendicularly crosses the horizontal axis at the period-averaged center of mass x_0, defined by Eq. (4.47). Therefore, while the reflection symmetry of individual drop profiles is generally broken, it still holds over the course of a period. This is not true for asymmetric modes (Fig. 4.17e), where the modulated traveling drop from Fig. 4.14b is used as an example in the comoving frame. Here, the displacement oscillates about zero asymmetrically, i.e., relation (4.49) is violated and spatial directions are not treated equally. In this case, this expresses the breaking of reflection symmetry by drift-pitchforks of standing waves. We note that in contrast, the anti-axisymmetric mode in Fig. 4.13 and Fig. 4.17d was *not* obtained from such a bifurcation but rather from a standard Hopf bifurcation of a symmetric, fully localized state.

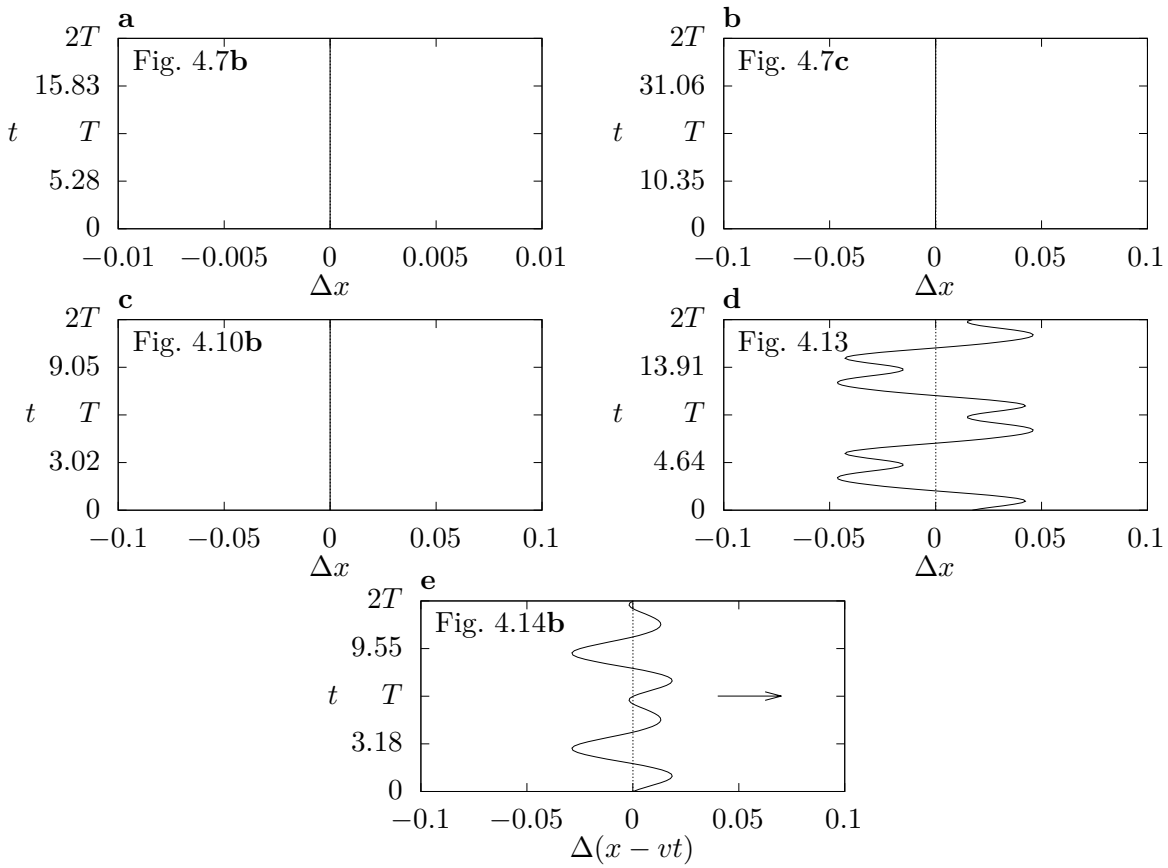

Figure 4.17: Space-time diagram of the displacement Δx for some of the previously shown solutions. The original solution plot is given in the top-left corner, **a-c** correspond to axisymmetric modes, **d** to an anti-axisymmetric mode and **e** to an asymmetric mode. In **e**, the state is considered in the comoving frame with speed v, the arrow indicates direction of travel. As a visual cue, a dashed base line is drawn.

5. Summary and Outlook

In the present thesis, a gradient dynamics approach was employed to study the interplay between bulk liquids and reactive surface dynamics. In particular, we considered a gradient dynamics based model for thin liquid films covered by insoluble surfactants in the presence of autocatalytic reactions and evaporation and studied the resulting (active) equations using the tools of linear stability analysis, time simulations and numerical continuation.

In chapter 2, the theoretical groundwork for a gradient dynamics description of reactive systems was laid. Based on the theory of non-equilibrium thermodynamics, general dynamical equations for non-equilibrium systems including chemical reactions were derived. In contrast to the usual assumption of linear laws which relate the thermodynamic fluxes and forces, an exponential relation was employed for chemical reactions to obtain mass action type kinetics. Based on the principle of detailed balance, we then showed that these dynamical equations possess a gradient dynamics structure, meaning that a corresponding Lyapunov-functional can be found. Then, some simple example systems were given as applications. It was also discussed in detail how the usual assumption of constant chemical concentrations breaks the gradient dynamics form and how non-equilibrium models like the Brusselator can be recovered.

In chapter 3 we dealt with the description of thin films of liquid that are covered by insoluble, reactive surfactants. First, by considering equilibrium drops an amended Young's law for drops covered by reactive, insoluble surfactants was found. Then, a consistency condition between the macroscopic and the mesoscopic description was derived. Finally, the dynamical equations were presented as a gradient dynamics, where we used the results from chapter 2. Here, we also discussed how the gradient dynamics form results in cross-coupling effects between wetting-related phenomena and chemical reactions, leading e.g. to a film height dependent reaction suppression.

In chapter 4, we used the results from chapter 3 to construct a model for non-equilibrium drops that are covered by surfactants which engage in an autocatalytic reaction and may transition between the gas phases and the drop surface by evaporation and condensation. The gas phases were assumed to be chemostatted to drive the drop away from thermodynamic equilibrium. First, we analyzed the linear stability of a flat film. It was seen that as the driving force increases in magnitude, the flat film becomes Hopf- and Turing-unstable and spatio-temporal pattern formation is facilitated. We then studied the model extensively using numerical continuation, supplemented by time simulations. Bifurcation diagrams of a simple drop revealed bifurcations of stationary drops with patterned surfactants which strikingly resemble the appearance of localized states in homoclinic snaking. Besides these patterned surfactant states, we also found distinct modes of drop oscillation, namely parity axisymmetric, anti-axisymmetric and asymmetric modes. The different mode types were classified using the dynamics of the drop center of mass. Here, it was discussed that axisymmetric and anti-axisymmetric modes obey reflection symmetry and "period-averaged" reflection symmetry, respectively. This is untrue for asymmetric modes, which emerge from parity-breaking drift-pitchfork bifurcations of standing waves. In the laboratory frame, these states correspond to modulated traveling drops. In the continuation and in time simulations, we found (linearly) stable traveling drops and modulated traveling drops. Therefore, the model was shown to allow for the directional transport of bulk liquid as a result of spontaneous symmetry breaking.

While the results from chapters 2 and 3 are of rather general nature, the model presented in chapter 4 can be extended in various ways. In the discussed model, interactions between the surfactants and the substrate were neglected. Considering the results from chapter 3, it may be interesting to study the influence of cross-coupling effects between wetting and chemical reactions on the observed drop dynamics. Additionally, the concrete analysis was carried out in one spatial dimension. As an extension, the model could be considered in a two-dimensional chan-

nel geometry. Here, it would be particularly interesting to study the coupling of the oscillatory modes and the traveling solutions to the system geometry, possibly leading to further control of liquid transport. Furthermore, we refrained from specifying the class of bifurcations from which the drops with patterned surfactants emerge. Here, further work is needed. In particular, it needs to be investigated how this bifurcation class is connected to general properties of the model, i.e. symmetries, how it relates to homoclinic snaking and how it depends on choices of parameters. In this regard, it will be interesting to see whether the specific form of the driving force is relevant to the occurrence of this bifurcation class since we employed symmetric driving terms, here.

A. Appendix

A.1 Some Intermediate Results

During the study of the model presented in chapter 4, multiple time simulation parameter scans were performed as an extension of the parameter scans employed in the linear stability analysis. The result of one these scans is shown in Fig. A.1.

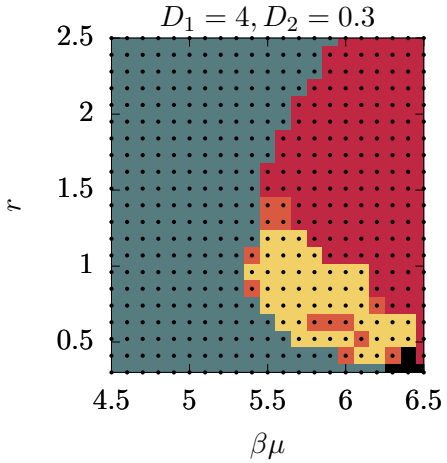

Figure A.1: Time simulation parameter scan of the model presented in chapter 4 on a periodic domain of $L = 500$. The parameters are $W = 8, \delta = 1, D_1 = 4, D_2 = 0.3, \beta_1 = 6, \beta_2 = 1$. Dots indicate scan points. Colors denote "qualitatively different" regimes. Black regions correspond to invalid data. As an initial condition, we used a perturbed drop with noisy surfactants.

Here, colors denote different "qualitatively different" regimes that were observed in the time simulations: relaxation to a simple drop (blue), axisymmetric drop oscillation (yellow), anti-axisymmetric drop oscillation (orange) and Turing patterned surfactants (red). These results were obtained by running the time simulations for a fixed run time (120 s) at each point of the scan and the data was evaluated manually. As an initial condition, we used a perturbed drop with noisy surfactants. While the shape of the transition line from a simple drop to self-organizing behavior roughly matches the results from the linear stability analysis, it is likely that some of the points were misclassified, as the run time for each point was chosen rather low and no quantitative measure was used to distinguish solution classes. In particular, some of the observed drop oscillations were most likely transients. Nevertheless, these results are still valuable since the "patches" of anti-axisymmetric modes within the region of axisymmetric modes suggest multistable properties which in turn gave the incentive to analyze the model using numerical continuation.

Bibliography

[Arg+05] M. Argentina et al. “Coarsening dynamics of the one-dimensional Cahn-Hilliard model”. In: *Phys. Rev. E* 71 (2005), p. 046210.

[BB18] F. Benfenati and G. P. Beretta. “Ergodicity, Maximum Entropy Production, and Steepest Entropy Ascent in the Proofs of Onsager’s Reciprocal Relations”. In: *J. Non-Equilib. Thermodyn.* 43 (2018), pp. 101–110.

[BCR89] P. A. J. de Boer, R. E. Crossley, and L. I. Rothfield. “A division inhibitor and a topological specificity factor coded for by the minicell locus determine proper placement of the division septum in E. coli”. In: *Cell* 56 (1989), pp. 641–649.

[BEK78] J. Bataille, D. G. B. Edelen, and J. Kestin. “Nonequilibrium Thermodynamics of the Nonlinear Equations of Chemical Kinetics”. In: *J. Non-Equilib. Thermodyn.* 3 (1978), pp. 153–168.

[Ber+08] A. Bergeon et al. “Eckhaus instability and homoclinic snaking”. In: *Phys. Rev. E* 78 (2008), p. 046201.

[BK07] J. Burke and E. Knobloch. “Homoclinic snaking: Structure and stability”. In: *Chaos* 17 (2007), p. 037102.

[Bra+21] F. Brauns et al. “Wavelength Selection by Interrupted Coarsening in Reaction-Diffusion Systems”. In: *Phys. Rev. Lett.* 126 (2021), p. 104101.

[Bur+22] T. Burkart et al. “Control of protein-based pattern formation via guiding cues”. In: *Nat. Rev. Phys.* 4 (2022), pp. 511–527.

[CGA22] M. W. Cotton, R. Golestanian, and J. Agudo-Canalejo. “Catalysis-Induced Phase Separation and Autoregulation of Enzymatic Activity”. In: *Phys. Rev. Lett.* 129 (2022), p. 158101.

[Che+21] A. G. Cherstvy et al. “Inertia triggers nonergodicity of fractional Brownian motion”. In: *Phys. Rev. E* 104 (2021), p. 024115.

[De 20] A. De Wit. “Chemo-Hydrodynamic Patterns and Instabilities”. In: *Annu. Rev. Fluid Mech.* 52 (2020), pp. 531–555.

[Don+20] C. Donau et al. “Active coacervate droplets as a model for membraneless organelles and protocells”. In: *Nat. Commun.* 11 (2020), p. 5167.

[FAT12] Ľ. Fraštia, A. J. Archer, and U. Thiele. “Modelling the formation of structured deposits at receding contact lines of evaporating solutions and suspensions”. In: *Soft Matter* 8 (2012), pp. 11363–11386.

[FDT91] S. Fauve, S. Douady, and O. Thual. “Drift instabilities of cellular patterns”. In: *J. Phys. II France* 1 (1991), pp. 311–322.

[Fei72] M. Feinberg. “Complex balancing in general kinetic systems”. In: *Arch. Ration. Mech. Anal.* 49 (1972), pp. 187–194.

[Fei87] M. Feinberg. “Chemical reaction network structure and the stability of complex isothermal reactors—I. The deficiency zero and deficiency one theorems”. In: *Chem. Eng. Sci.* 42 (1987), pp. 2229–2268.

[Fit61] R. FitzHugh. “Impulses and Physiological States in Theoretical Models of Nerve Membrane”. In: *Biophys. J.* 1 (1961), pp. 445–466.

[Flo42] P. J. Flory. “Thermodynamics of High Polymer Solutions”. In: *J. Chem. Phys.* 10 (1942), pp. 51–61.

[FT23] T. Frohoff-Hülsmann and U. Thiele. *Nonreciprocal Cahn-Hilliard model emerges as a universal amplitude equation*. 2023. arXiv: `2301.05568 [nlin.PS]`.

[FWT21] T. Frohoff-Hülsmann, J. Wrembel, and U. Thiele. “Suppression of coarsening and emergence of oscillatory behavior in a Cahn-Hilliard model with nonvariational coupling”. In: *Phys. Rev. E* 103 (2021), p. 042602.

[Gas22] P. Gaspard. *The Statistical Mechanics of Irreversible Phenomena*. Cambridge University Press, 2022.

[GBQ04] P.-G. de Gennes, F. Brochard-Wyart, and D. Quéré. *Capillarity and Wetting Phenomena: Drops, Bubbles, Pearls, Waves*. Springer, 2004.

[Gla+09] K. Glasner et al. “Ostwald ripening of droplets: The role of migration”. In: *Eur. J. Appl. Math.* 20 (2009), pp. 1–67.

[Gol+91] R. E. Goldstein et al. “Hydrodynamic and interfacial patterns with broken space-time symmetry”. In: *Phys. Rev. A* 43 (1991), pp. 6700–6721.

[Gor14] A.N. Gorban. “Detailed balance in micro- and macrokinetics and micro-distinguishability of macro-processes”. In: *Results Phys.* 4 (2014), pp. 142–147.

[Har+23] S. Hartmann et al. “Sessile drop evaporation in a gap – crossover between diffusion-limited and phase transition-limited regime”. In: *J. Fluid Mech.* 960 (2023), A32.

[Hei17] T. Heimburg. “Linear nonequilibrium thermodynamics of reversible periodic processes and chemical oscillations”. In: *Phys. Chem. Chem. Phys.* 19 (2017), pp. 17331–17341.

[HF18] J. Halatek and E. Frey. “Rethinking pattern formation in reaction–diffusion systems”. In: *Nat. Phys.* 14 (2018), pp. 507–514.

[HH06] M. Heil and A. L. Hazel. “oomph-lib – An Object-Oriented Multi-Physics Finite-Element Library”. In: *Fluid-Structure Interaction*. Ed. by Hans-Joachim Bungartz and Michael Schäfer. Berlin, Heidelberg: Springer Berlin Heidelberg, 2006, pp. 19–49.

[HH52] A. L. Hodgkin and A. F. Huxley. “A quantitative description of membrane current and its application to conduction and excitation in nerve”. In: *J. Physiol.* 117 (1952), pp. 500–544.

[HJ72] F. Horn and R. Jackson. “General mass action kinetics”. In: *Arch. Ration. Mech. Anal.* 47 (1972), pp. 81–116.

[HK09] S. M. Houghton and E. Knobloch. “Homoclinic snaking in bounded domains”. In: *Phys. Rev. E* 80 (2009), p. 026210.

[Hug41] M. L. Huggins. “Solutions of Long Chain Compounds”. In: *J. Chem. Phys.* 9 (1941), pp. 440–440.

[Ian+22] A. Ianeselli et al. “Non-equilibrium conditions inside rock pores drive fission, maintenance and selection of coacervate protocells”. In: *Nat. Chem.* 14 (2022), pp. 32–39.

[JBT05] K. John, M. Bär, and U. Thiele. “Self-propelled running droplets on solid substrates driven by chemical reactions”. In: *Eur. Phys. J. E* 18 (2005), pp. 183–199.

[Köp+10] M. H. Köpf et al. “Pattern Formation in Monolayer Transfer Systems with Substrate-Mediated Condensation”. In: *Langmuir* 26 (2010), pp. 10444–10447.

[KZ21] J. Kirschbaum and D. Zwicker. “Controlling biomolecular condensates via chemical reactions”. In: *J. R. Soc. Interface* 18 (2021), p. 20210255.

[Nic95] G. Nicolis. *Introduction to Nonlinear Science*. Cambridge University Press, 1995.

[Ons31a] L. Onsager. “Reciprocal Relations in Irreversible Processes. I.” In: *Phys. Rev.* 37 (1931), pp. 405–426.

[Ons31b] L. Onsager. “Reciprocal Relations in Irreversible Processes. II.” In: *Phys. Rev.* 38 (1931), pp. 2265–2279.

[Per+07] A. Pereira et al. “Dynamics of a horizontal thin liquid film in the presence of reactive surfactants”. In: *Phys. Fluids* 19 (2007), p. 112102.

[Pri47] I. Prigogine. *Étude thermodynamique des phénomènes irréversibles*. Paris: Dunod, 1947.

[RM61] J. Ross and P. Mazur. “Some Deductions from a Formal Statistical Mechanical Theory of Chemical Kinetics”. In: *J. Chem. Phys.* 35 (1961), pp. 19–28.

[SP84] S. R. de Groot and P. Mazur. *Non-Equilibrium Thermodynamics*. New York: Dover Publications, Inc., 1984.

[TAP12] U. Thiele, A. J. Archer, and M. Plapp. “Thermodynamically consistent description of the hydrodynamics of free surfaces covered by insoluble surfactants of high concentration”. In: *Phys. Fluids* 24 (2012), p. 102107.

[TAP16] U. Thiele, A. J. Archer, and L. M. Pismen. “Gradient dynamics models for liquid films with soluble surfactant”. In: *Phys. Rev. Fluids* 1 (2016), p. 083903.

[Thi+18] U. Thiele et al. “Equilibrium Contact Angle and Adsorption Layer Properties with Surfactants”. In: *Langmuir* 34 (2018), pp. 7210–7221.

[TJB04] U. Thiele, K. John, and M. Bär. “Dynamical Model for Chemically Driven Running Droplets”. In: *Phys. Rev. Lett.* 93 (2004), p. 027802.

[Tri18] S. Trinschek. “Thin-Film Modelling of Complex Fluids and Bacterial Colonies”. PhD thesis. Westfälische Wilhelms-Universität Münster, 2018.

[Tur52] A. M. Turing. “The chemical basis of morphogenesis”. In: *Phil. Trans. R. Soc. Lond. B* 237 (1952), pp. 37–72.

[Uec21] H. Uecker. *Numerical Continuation and Bifurcation in Nonlinear PDEs*. Philadelphia, PA: Society for Industrial and Applied Mathematics, 2021.

[Weg02] R. Wegscheider. “Über simultane Gleichgewichte und die Beziehungen zwischen Thermodynamik und Reaktionskinetik homogener Systeme”. In: *Z. Phys. Chem.* 39U (1902), pp. 257–303.

[Wil16] M. Wilczek. “Pattern Formation in Driven Thin Layers of Simple and Complex Liquids”. PhD thesis. Westfälische Wilhelms-Universität Münster, 2016.

[You05] T. Young. “III. An essay on the cohesion of fluids”. In: *Phil. Trans. R. Soc.* 95 (1805), pp. 65–87.

[Zwi+17] D. Zwicker et al. “Growth and division of active droplets provides a model for protocells”. In: *Nat. Phys.* 13 (2017), pp. 408–413.

[Zwi22] D. Zwicker. “The intertwined physics of active chemical reactions and phase separation”. In: *Curr. Opin. Colloid Interface Sci.* 61 (2022), p. 101606.

Declaration of Academic Integrity

I hereby confirm that this thesis, entitled "Gradient Dynamics Approach to Chemically Reacting Sessile Liquid Drops", is solely my own work and that I have used no sources or aids other than the ones stated. All passages in my thesis for which other sources, including electronic media, have been used, be it direct quotes or content references, have been acknowledged as such and the sources cited. I am aware that plagiarism is considered an act of deception which can result in sanction in accordance with the examination regulations.

12.09.2023 - E. V.

(date, signature of student)

I consent to having my thesis cross-checked with other texts to identify possible similarities and to having it stored in a database for this purpose.

I confirm that I have not submitted the following thesis in part or whole as an examination paper before.

12.09.2023 - E. V.

(date, signature of student)